

Science with the

# Constellation-X

Observatory

supernovae

**black holes**

**life cycles of matter in the universe**

**dark matter clusters of galaxies extreme gravity**

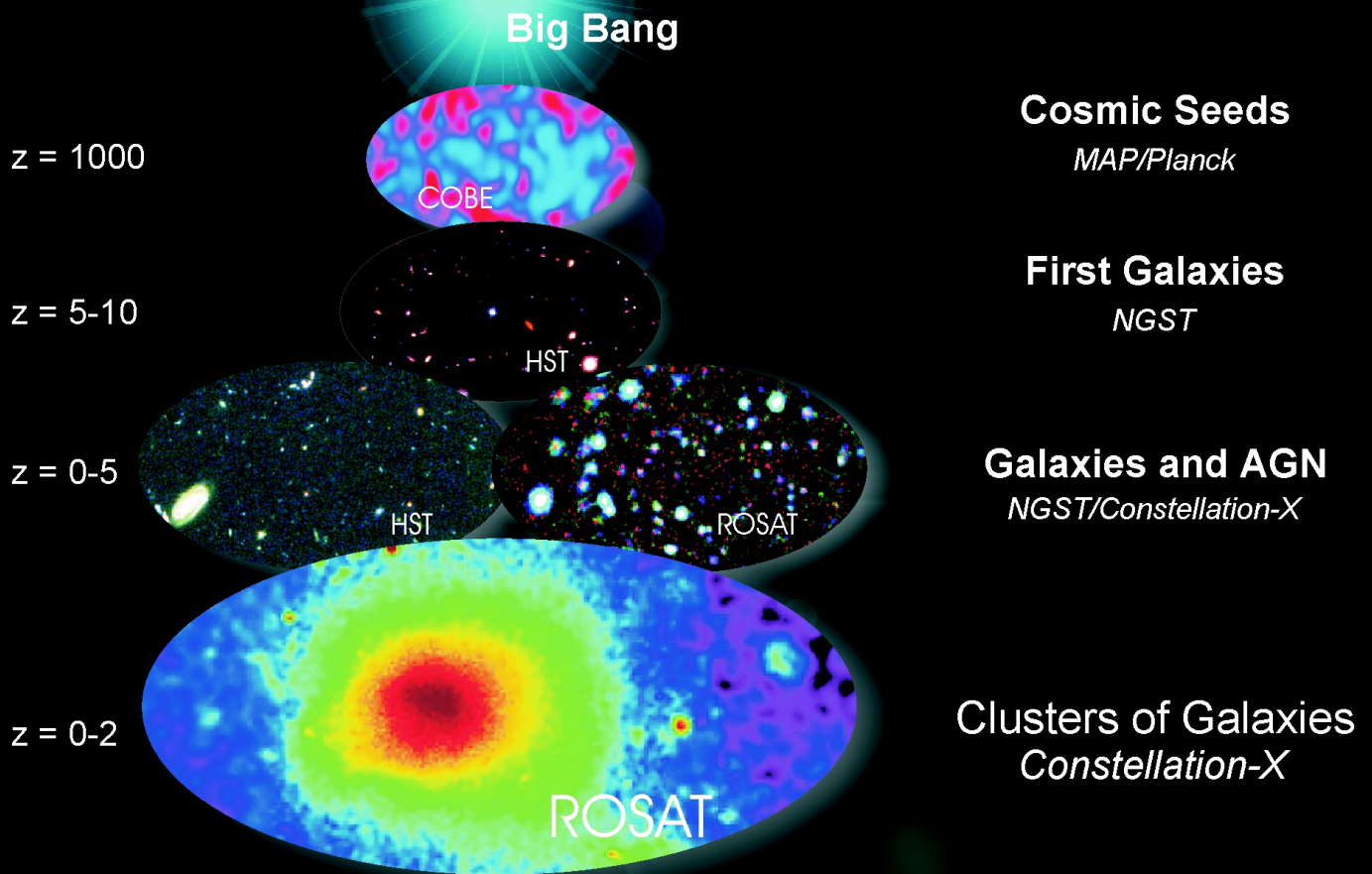
**cosmic jets stellar coronae neutron stars**

**white dwarfs**

June 1999

<http://constellation.gsfc.nasa.gov/>

# Structure in the Universe



Models of the Universe aim to account for the properties of all structure, from the fluctuations in the microwave background to the formation of the first galaxies and clusters of galaxies, the largest structures in the Universe. Hierarchical cosmological models predict that the largest structures formed most recently; however, the time of their appearance critically depends on the assumed cosmology. MAP and Planck will study in detail the fluctuations in the microwave background. The Next Generation Space Telescope (NGST) will zoom in on the first galaxies as they appear at high redshift. At intermediate redshift, Constellation-X and NGST will study the evolution of AGN and starburst galaxies. In addition, Constellation-X will also address fundamental questions related to the formation epoch and evolution of the largest structures, the clusters of galaxies.

*On the cover: Artist's concept of a galaxy with an active nucleus, containing a supermassive black hole that is surrounded by a disk of accreting material. Two narrow jets are seen coming from the nucleus. The powerful radiation that we observe in quasars and active galaxies is sustained by the accretion disk, which feeds matter directly onto the black hole. By detecting the signature of energy loss by photons that are under the extreme pull of gravity, Constellation-X will probe regions close to the event horizon of the central black hole.*

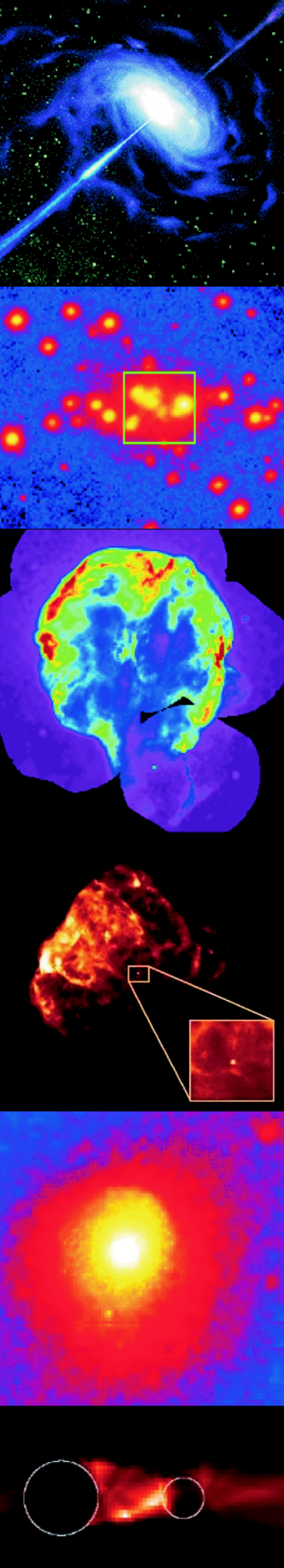


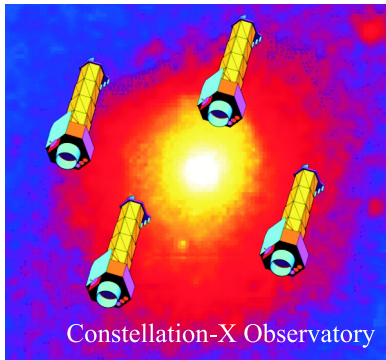
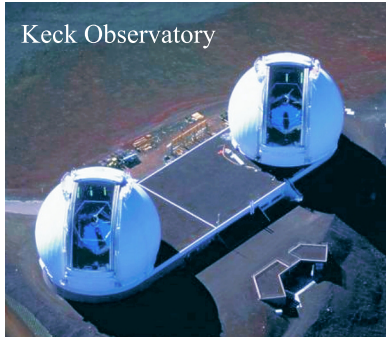
# Table of contents

Executive Summary . . . . .	1
1 Science Goals . . . . .	3
1.1 Decade of Discovery . . . . .	3
1.2 The Ultimate Limits of Gravity . . . . .	4
1.3 The Evolving Universe . . . . .	6
2 Constellation-X . . . . .	9
2.1 X-ray Astronomy Comes of Age . . . . .	9
2.2 Mission Implementation . . . . .	9
2.2.1 Effective Area . . . . .	9
2.2.2 Spectral Resolution . . . . .	11
2.2.3 Bandpass . . . . .	13
3 Example Mission Science . . . . .	15
3.1 Matter Under Extreme Gravity . . . . .	15
3.1.1 Supermassive Black Holes . . . . .	15
3.1.2 Stellar Endpoints . . . . .	20
3.2 Life Cycles of Matter in the Evolving Universe . . . . .	24
3.2.1 Galaxy Clusters and the Intracluster Medium . . . . .	24
3.2.2 Galaxies and the Intergalactic Medium . . . . .	26
3.2.3 Stars, Supernovae, and the Interstellar Medium . . . . .	29
3.2.4 Solar System X-rays . . . . .	33
4 The Technology . . . . .	35
4.1 Introduction . . . . .	35
4.2 Spectroscopy X-ray Telescopes . . . . .	35
4.2.1 Replicated Shells . . . . .	36
4.2.2 Replicated Foil Segments . . . . .	36
4.2 Calorimeters . . . . .	37
4.3 Gratings/CCD Arrays . . . . .	39
4.4 Hard X-ray Telescope (HXT) Systems . . . . .	40
4.5 Mission Description . . . . .	41
4.5.1 GSFC/SAO Baseline Configuration . . . . .	42
4.5.2 TRW Baseline Configuration . . . . .	42
4.5.3 Ball Aerospace Baseline Configuration . . . . .	43
References . . . . .	45
Acknowledgments . . . . .	47



# Executive Summary

## High Resolution Spectroscopy



The Constellation X-Ray Mission is a high throughput X-ray facility emphasizing observations at high spectral resolution ( $E/\Delta E \sim 300-3000$ ) while covering a broad energy bandpass (0.25–40 keV). Constellation-X will provide a factor of nearly 100 increase in sensitivity over current high resolution X-ray spectroscopy missions and, in so doing, will obtain high quality spectra for all classes of X-ray sources over a wide range of luminosity and redshift. It is the X-ray astronomy equivalent of large ground-based optical telescopes such as the Keck Observatory and the ESO Very Large Telescope.

Constellation-X is a key element in NASA's Structure and Evolution of the Universe (SEU) theme aimed at understanding the great mysteries of space, time, and energy. When observations commence towards the end of the next decade, Constellation-X will address many pressing questions concerning the extremes of gravity and the evolution of the Universe. X-ray observations of broadened iron emission lines in Active Galactic Nuclei will measure black hole masses and spins and will test General Relativity in the strong gravity limit. Constellation-X will show us how black holes evolve with cosmic time and, as accretion energy may be a dominant component, will provide critical information on the total energy output of the Universe. By looking across a broad range of redshift, Constellation-X will reveal the earliest formation of clusters of galaxies and tell us whether their properties are consistent with current models of galaxy formation. Present inventories indicate that many of the baryons predicted by Big Bang nucleosynthesis and subsequent stellar processing seem to be "missing," and Constellation-X will allow us to search for them—for example, in a hot, metal-enriched Intergalactic Medium.

Exploring and expanding our cosmic horizons requires sensitive X-ray observations. This document is intended for scientists. It describes the Constellation-X science goals and mission capabilities and portrays the science that can be achieved. Constellation-X is envisioned as an international facility, open to all scientists.



# 1 Science Goals

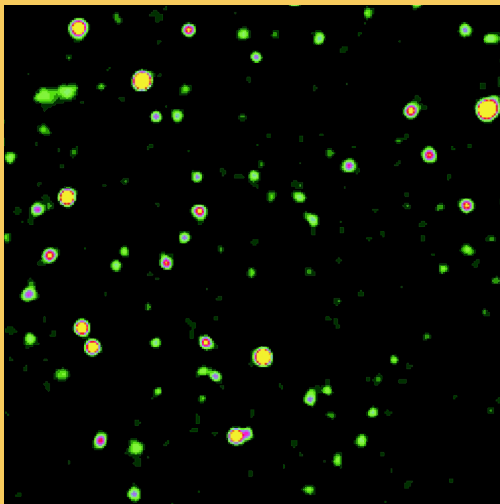
*New Windows on the Universe . . .*

## 1.1 Decade of Discovery

A major goal of science is to understand how our Universe arrived at its present state and to understand its ultimate destiny. Over the past decade, astronomy has been revolutionized by observing with large ground-based telescopes, such as the 10 m Keck Observatory, and by observing from space, away from the effects of the Earth's atmosphere. As a result, the entire electromagnetic spectrum has been opened to exploration and new discoveries have been made at an increasingly fast pace. For instance, the Cosmic Background Explorer (COBE) found the first observational link between the origin of structure shortly after the Big Bang and the structure we see today. The Hubble Space Telescope (HST) and the Keck Observatory found very young galaxies at a redshift of 5. The Compton Gamma Ray Observatory (CGRO) discovered gamma-ray blazars. BeppoSAX, CGRO, and the Keck revealed that the most energetic explosions in the Universe are not supernova, as once thought, but rather gamma-ray bursts that may involve the catastrophic creation of black holes at high redshift. The Advanced Satellite for Cosmology and Astrophysics (ASCA) measured a relativistically broadened iron  $K\alpha$  emission line from active galactic nuclei (AGN), a signature of strong general relativistic effects that provides a new probe of the immediate black hole environment. The X-ray satellite ROSAT resolved 80% of the X-ray background at 1 keV into discrete sources, many of which are AGN at high redshift. The Rossi X-ray Timing Explorer (RXTE) discovered a rich spectrum of millisecond oscillations and pulsations from the vicinity of neutron stars and black holes in X-ray binaries. While these are just a few examples of the fantastic discoveries of the last decade, the future is even brighter. As technology advances, even more capable telescopes can be built to carry forward the pace of discovery.

Over the past 35 years, X-ray astronomy has grown from infancy to near-maturity and is now an indispensable tool poised at the cutting edge of astrophysical research. One reason for this is that X-ray observations reveal some of the most energetic phenomena in the Universe. They provide sensitive probes of astrophysical plasmas at or above temperatures of a million degrees and are the best means of investigating atomic and nuclear processes in the kilovolt range. Hence, X-ray astronomy is crucial for the study of the most fundamental questions in astrophysics involving high temperatures or explosions.

Constellation-X is a high spectral resolution, large aperture X-ray mission that is currently under design. This volume describes the mission, with an emphasis on science goals and their feasibility. In the rest of this Section, fundamental science questions are discussed. Section 2 describes Constellation-X and its capabilities. Section 3 presents a sample of scientific problems that will be addressed with this X-ray observatory ranging from studies of stellar coronae and supernova remnants to black holes and stellar endpoints, from clusters of galaxies to active galactic nuclei and from the interstellar to the intergalactic medium. Finally, Section 4 is devoted to the mission technology.



### **ROSAT Deep Field**

Thirty-five years after discovery of the Cosmic X-ray Background, ~80% of the background at 1 keV has been resolved into discrete sources by ROSAT, from surveys that reach a factor of 10 deeper than the Einstein deep fields. This  $25' \times 25'$  image taken by the ROSAT High Resolution Imager (million second exposure) shows the Lockman hole region. It is the deepest X-ray image of the sky achieved so far. (Hasinger et al., 1998)

Optical identification programs for the ROSAT sources reveal that many are AGN at a mean redshift of 1.5, reaching out to redshifts as high as 4, with no evidence for a decline in the X-ray selected QSO population towards higher  $z$  (Miyaji et al., 1998). Constellation-X will be able to take detailed high resolution spectra from the brightest to the faintest sources in the exposure pictured here.

## 1.2 The Ultimate Limits of Gravity

Since their discovery, quasars and active galactic nuclei (AGN) have stood out as uniquely luminous objects in the Universe. Today we are confident that their ultimate power source is the release of gravitational energy sustained by an accretion disk, which is feeding matter directly into a central supermassive black hole. Such black holes appear to reside at the centers of most galaxies, and they have masses of millions to billions times that of our Sun. However, the manner in which the accreting material reaches the black hole and the mechanism for the production of electromagnetic radiation and jets from this material remain unclear.

Radio maser and HST observations probe regions located many hundreds of Schwarzschild radii from the black hole. Only in the X-ray band does the emission come from close to the event horizon. The hard X-ray emission of AGN is thought to arise from flares in a hot corona associated with the accretion disk. Some fraction of these X-rays illuminate the underlying accretion disk and the subsequent reflection imprints atomic features onto the observed spectrum. These features (specifically, the broad iron  $K\alpha$  line) are strongly distorted by gravitational effects and so provide a powerful probe of the physics of the accretion flow as well as the space-time geometry close to the black hole.

The high throughput and broad-band response of Constellation-X will allow us to utilize the iron-line diagnostic in an unprecedented manner. Observations of many individual sources will allow us to develop a statistical picture of the material surrounding the central black hole. We will search for abundance changes in this material as a function of look-back time and study details of chemical evolution in AGN. We will also determine the distribution of black hole masses and spins as functions of cosmic time. These data will reveal the underlying evolutionary processes and timescales as well as the connections between high-luminosity quasars and lower-luminosity Seyfert Galaxies.

### *How can we use observations of black holes to test General Relativity?*

Since supermassive black holes represent the most extreme gravitational environments known, the distortions of time and space predicted by general relativity are most pronounced in the vicinity of these objects. The broad iron  $K\alpha$  emission lines recently discovered by the ASCA Observatory for many X-ray bright AGN appear to be broadened by relativistic effects (Figure 1), indicating that much of the line emission originates close to the event horizon. This spectral feature provides a new diagnostic that Constellation-X will use to map out the geometry of the inner emission regions and determine the extent to which we can test general relativity. Such X-ray observations directly probe physical conditions close to the central engine and provide the ONLY way to determine black hole spin, which Constellation-X should be able to do for a large sample of AGN (Reynolds and Begelman, 1997).

### *What is the total energy output of the Universe?*

Until recently, less attention has been given to sources of energy in the Universe that are not directly visible at optical-UV wavelengths. However, the first observations of the hard X-ray sky by ASCA and BeppoSAX have revealed that many AGN are heavily absorbed, with their central engines primarily visible via hard X-rays (and perhaps via their infrared output as well). This picture is consistent with models for the X-ray background being made up of many absorbed AGN (Madau, Ghisellini, and Fabian, 1994). It also highlights the importance of the hard ( $> 10$  keV) X-ray band for studying the total energy

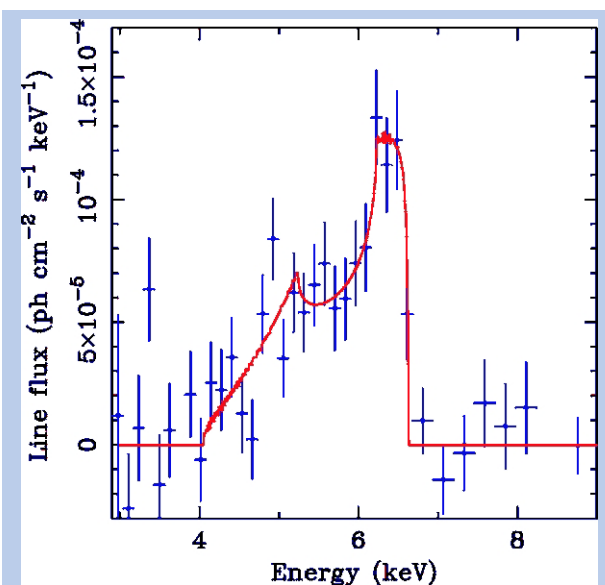
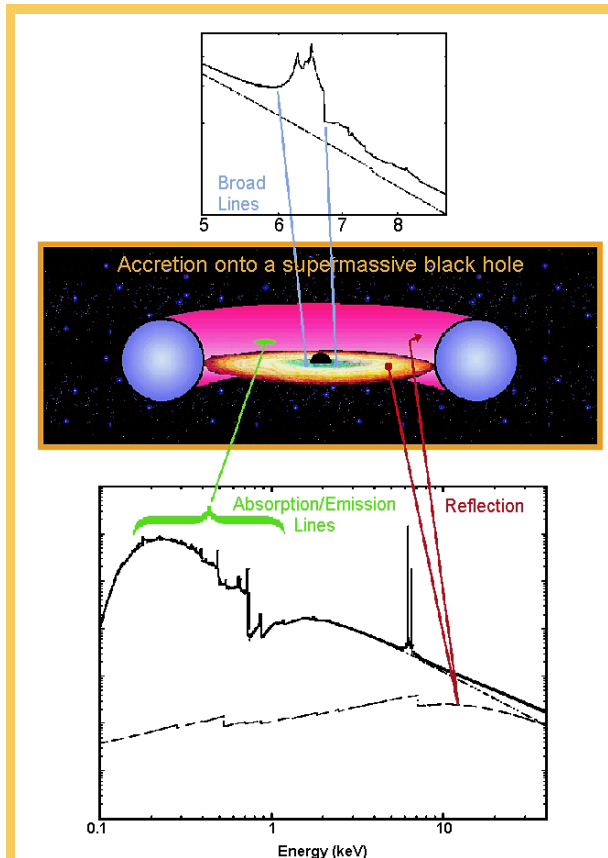


Figure 1. Very broad and asymmetric iron line profile as seen in a long ASCA observation of the Seyfert galaxy MCG-6-30-15 (Tanaka et al., 1995). The solid line is a model consisting of fluorescent emission from an accretion disk with an inclination of  $30^\circ$  around a non-rotating black hole. Much of the redshifted emission comes from within six Schwarzschild radii, i.e., close to the black hole event horizon.

output for these objects. The total accretion energy released by AGN may, in fact, be comparable to the energy generated by nuclear burning in the total stellar population, but in the former case, the central luminosity may be mostly hidden behind obscuring starburst regions within 100 pc of the AGN (Fabian et al., 1998). If most of the accretion in the Universe is highly obscured, then the emitted power per galaxy based on currently available optical, UV, or soft X-ray quasar luminosity functions may be substantially underestimated. By using hard X-ray spectra to advance our knowledge of the total luminosity of AGNs, Constellation-X will bring us closer to knowing the total energy output of the Universe.



The middle panel shows a schematic diagram of the innermost region of a Seyfert galaxy, which consists of a supermassive black hole surrounded by an accretion disk and optically-thick torus. The upper panel shows the iron  $K\alpha$  line at 6.4 keV that is produced in the innermost region of the accretion disk. Its profile is distorted by extreme gravitational and kinematic effects. Measurement of the profile allows us to probe the immediate environment of the black hole and to determine the black hole spin and mass.

The lower panel shows a broad-band perspective. When the AGN system is viewed face on (i.e., a Seyfert I), ionized gas along the line-of-sight imprints absorption edges and emission lines onto the intrinsic power-law continuum. The effects of such ionized gas are mostly visible in the X-ray band and the spectroscopic capabilities of Constellation-X will provide the detailed kinematic and plasma diagnostics necessary to determine its relationship to the accretion process. A hardening of the spectrum above  $\sim 7$  keV is produced by Compton "reflection" of the intrinsic continuum within the disk and torus. The sensitivity of Constellation-X, extending to high energies, provides an independent measure of the geometry and composition of these regions.

### *What roles do supermassive black holes play in galaxy evolution?*

While black holes may be ubiquitous in the nuclei of galaxies, their origins, evolution, and impact on galaxy evolution are not well understood. Quasars and related AGN provide important clues via their X-ray emission. The X-ray band above a few keV, like the far infrared, is relatively immune to obscuration and thus allows a unique view of AGN properties at high redshift. Optical samples suggest that AGN activity peaked at a redshift of 2–3, falling off before the peak of star forming activity (at  $z \sim 1.5$ ). On the other hand, discrete sources comprising 80% of the X-ray background at 1 keV in deep-field ROSAT observations (Hasinger et al., 1998) are mostly AGN, with a mean redshift of 1.5. In contrast to the optical samples, these X-ray selected quasars, which extend to redshifts as high as 4, show no evidence for a decline in the population towards higher  $z$  (Miyaji et al., 1998). We can predict confidently that as many as 1 million new AGN will be discovered by the Chandra and XMM X-ray observatories (scheduled to be launched in 1999 and 2000, respectively), providing an unbiased sample of AGN at  $z > 1$ . Constellation-X measurements of black hole mass and spin for selected subsets of this high  $z$  quasar sample will provide essential information comparing the properties of massive black holes to the evolution of their host galaxies, addressing questions such as: How do massive black holes at  $z \sim 3$  compare in mass and spin with those in the local Universe? Do massive black holes form when galaxies form, or do they form later? What are the relative evolution rates of black holes and their host galaxies?

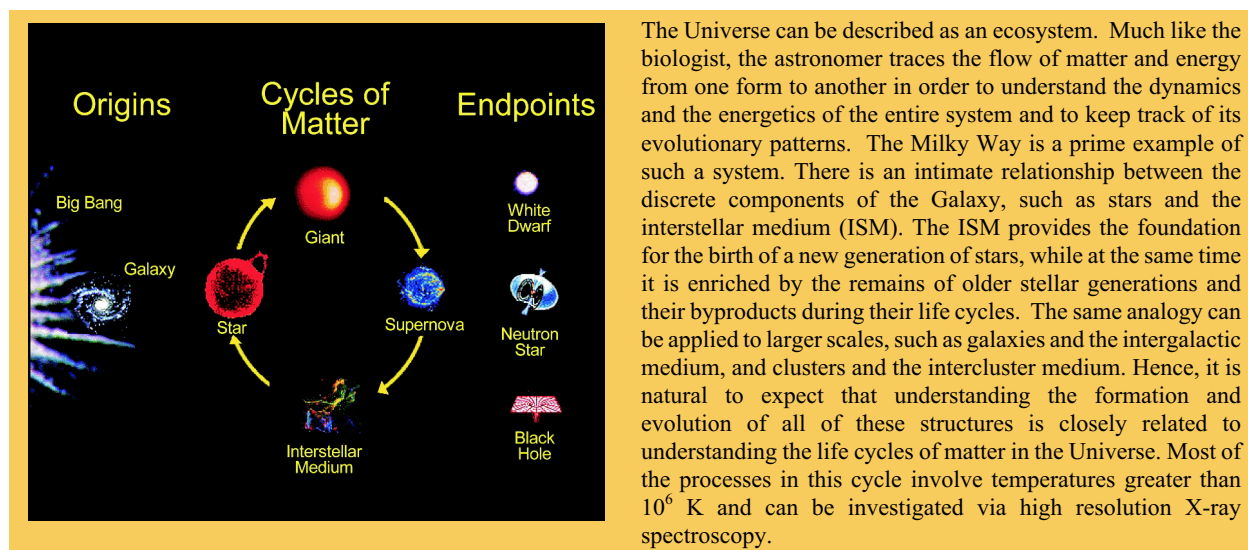
### *How does gas flow in accretion disks and how do cosmic jets form?*

Accretion disks play a fundamental role in many astrophysical settings, ranging from the formation of planetary systems to accretion onto supermassive black holes in AGN. They provide a mechanism to release gravitational energy that is 10 times more efficient than nuclear burning. Because of this, the study of accretion

disks is now a cornerstone of astrophysics. But in spite of much progress since the seminal papers of Shakura and Sunyaev (1973), Pringle and Rees (1972), and Lynden-Bell (1969), the basic workings of accretion disks remain puzzling. There are debates and controversies about the nature of viscosity which drives the accretion process, about the stability of the disk at various accretion rates, about the relevance of advection and mass outflows, and about the mechanisms by which jets are formed.

The most amenable places to study basic accretion physics are nearby systems within our own galaxy, such as cataclysmic variables and X-ray binaries, in which the X-ray, UV, and optical output is often dominated by emission from the disk. Optically-thick disks produce very soft spectra whereas optically-thin disks can become extremely hot. High sensitivity and high resolution Constellation-X spectral observations of X-ray novae and dwarf novae in quiescence, when the mass flow through the disk appears to be much reduced, can help unravel the nature of viscosity and the disk instabilities. Micro-quasars, in which superluminal motion is driven by jets, have been found in X-ray binaries in our Galaxy and may also hold clues as to how disks form. Examining the spectra of these objects over a wide range of luminosity will probe the physics of accretion disks to a level of detail not currently possible. This will be accomplished by resolving line features from the accretion disk photosphere and by measuring the continuum shape over a broad energy band.

### 1.3 The Evolving Universe



Since the discovery in the 1970s of massive clouds of hot gas filling the space between the galaxies in clusters (and groups), astronomers have come to realize the importance of these systems for studying cosmic evolution. Today we are confident that the baryonic content of clusters is dominated by the hot X-ray emitting gas, which also can be used to trace the overall mass content, including dark matter. We have also detected in clusters the presence of emission lines from highly ionized elements, particularly iron and oxygen, providing a powerful tool with which to study global nucleosynthesis as a function of redshift or cosmic time. However, we still have an incomplete understanding of the detailed physics, ranging from nuclear processing during stellar evolution and supernova explosions to galactic winds feeding the intracluster medium (ICM) and the intergalactic medium (IGM) to the importance of galaxy collisions, mergers, and ram-pressure stripping for determining the structure and content of clusters.

The gas temperature of essentially all virialized systems is in excess of one million degrees and thus requires X-ray observations to extract and exploit this wealth of information. Similarly, X-ray data are essential for probing the low redshift intergalactic medium to search for the “missing” local baryons via oxygen emission lines and via absorption features imprinted on spectra of background objects (such as quasars) by the metals in the IGM.

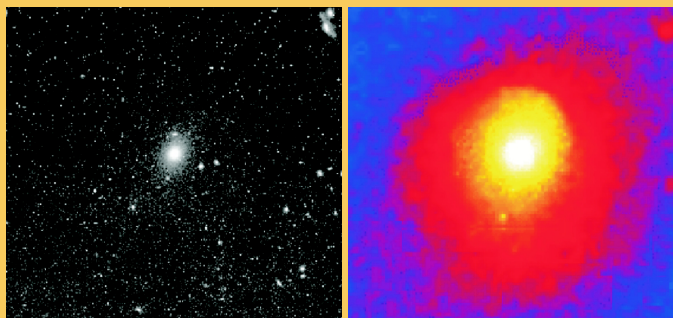
The high throughput, high energy resolution, and spatially resolved spectroscopy provided by Constellation-X will allow us to determine cluster abundances and internal velocity dynamics with sufficient precision to study cluster

formation and evolution over a wide range of redshift. The same capabilities enable us to study supernova remnants and to understand the supply of enriched material to the interstellar medium (ISM), ICM, and IGM. The high throughput and spectral resolution are essential for probing the contents of the IGM and searching for the remainder of the baryons not found in galaxies or the ICM.

#### *When were clusters of galaxies formed and how do they evolve?*

The hot ICM dominates the baryonic mass content of clusters of galaxies—the largest known gravitationally organized systems. Measurements of both the bremsstrahlung continuum and collisionally excited resonance emission lines trace the integrated results of stellar nucleosynthesis, the dispersal of heavy elements into the ISM via stellar winds and supernova explosions, and the feeding of enriched material into the ICM by galactic winds and mergers as we look back over cosmic time.

Shown are emissions from the Virgo Cluster of Galaxies in optical (left) and X-ray (right). In the optical, a bright central elliptical galaxy is surrounded by a cluster of similar galaxies. In contrast, the X-ray image shows a large ball of hot gas, the mass of which exceeds that of all of the Virgo galaxies by several factors. This gas is trapped by dark matter which in turn dominates the overall system mass. X-ray observations are crucial to map the mass content, metal abundances, and velocity profile of the cluster.



To date, cluster abundances have been measured in the X-ray band out to a redshift of about 0.4 showing the relative contributions from Type 1 and Type 2 supernova explosions but no discernible evolution with  $z$ . Constellation-X spectra of clusters over a range of redshifts, including those discovered by Chandra and XMM at high  $z$ , will provide crucial information about the presence of primordial gas, including any input from possible pre-galactic generations of stars as well as the contribution from stellar nucleosynthesis as a function of time. The high sensitivity of Constellation-X is essential for extending such studies to the “poorer cousins” of clusters, groups of galaxies.

By mapping the velocity distribution of hot cluster gas via Doppler shifts in the emission lines, Constellation-X will allow us to examine the dynamics within the cluster and specifically to study the effects of collisions and mergers between member galaxies and between separate subclusters and clusters. If, as expected, upcoming observations with Chandra and XMM indicate complex temperature distributions for cluster gas as well as an absence of hydrostatic equilibrium (due, for example, to frequent merging activity), then Constellation-X measurements of velocity distributions and dynamics will be required for accurate maps of the overall mass content and distribution of both luminous and dark matter in clusters and groups. Such information is essential for determining the overall baryonic and non-baryonic mass content of the Universe and for addressing a wide range of cosmological questions from Big Bang nucleosynthesis to the expansion rate and eventual fate of the Universe. Upcoming missions such as MAP and Planck will also address these questions but from an independent perspective.

#### *Where are the "missing baryons" in the local Universe?*

Recent observations of the Lyman- $\alpha$  forest show that at large redshifts most of the predicted baryon content of the Universe is in the IGM. However, at lower redshifts Fukugita, Hogan, and Peebles (1998) have shown that the baryon content of stars, neutral hydrogen, and X-ray emitting cluster gas is roughly one order of magnitude less than expected. In fact, a large fraction of the baryonic content in the local Universe has yet to be detected and can therefore be considered “missing.” Numerical simulations of formation and evolution of structure in the Universe now predict that a significant amount of low redshift, baryonic material may reside in the IGM with a temperature range of  $10^5$ – $10^7$  K (Cen and Ostriker, 1998). We expect H, He, and other elements with low ionization potential to be highly ionized in such a medium and therefore unable to produce detectable absorption lines in the optical or ultraviolet bands. Such gas

in the IGM can be detected with the high sensitivity, high resolution instruments aboard Constellation-X through OVII and OVIII emission lines and through the absorption lines of metals against the X-ray spectra of background quasars.

*How are matter and energy exchanged between stars and the Interstellar Medium and how is the Intergalactic Medium enriched?*

The ISM is a complex system of mutually interacting gas, dust, cosmic rays, and magnetic fields. After the Big Bang, the chemical evolution of the Universe was dominated by stellar formation, nucleosynthesis in stars, and the release of the processed material into the ISM via stellar winds and supernova explosions. X-ray spectroscopy of shock-heated plasmas in supernova remnants is thus an essential tool for investigating this entire process and solving many of the remaining mysteries. Detailed, spatially-resolved X-ray spectra reveal the stellar/supernova abundances, the composition of the surrounding ISM (possibly enriched by the stellar wind prior to the supernova explosion), and the interaction of the expanding blast wave with the surrounding material. Moreover, supernova explosions and enhanced star forming activities can drive hot gas out of a galaxy. These starburst-drive winds can enrich the ICM and/or IGM (depending on a galaxy's environment) on megaparsec scales.

Measurements of the higher energy continuum spectra of young supernova remnants will also provide crucial information on the possible sites for cosmic ray acceleration. CCDs like those on ASCA, Chandra, XMM, and Astro-E will provide sufficient spectral resolution to measure abundances of the more common elements such as O, Ne, Mg, Si, S, Ar, Ca, and Fe, but the higher throughput of Constellation-X is essential to measure the K-lines of elements such as F, Na, Al, P, Cl, K, Sc, Ti, V, Cr, Mn, Co, Ni, Cu, and Zn. Such data will go beyond the classification of the type of supernova explosion to put extensive constraints on nucleosynthesis models and will be combined with models of stellar formation and evolution to determine the integrated sum of enriched material returned to the ISM. The increased sensitivity of Constellation-X will allow us to extend these studies to external galaxies, beyond the Magellanic Clouds to M31 and M33, for example, to allow us to further our understanding of the history of star formation and the exchanges of matter between the ISM and stars. We expect to use the insight gained from such studies to generate predictions for the content of the ICM and IGM, which will refine the various models and further our understanding of this complex cycle.

*What is the role of magnetic fields in stellar evolution?*

The origin of stellar magnetic fields, thought to be due to the workings of a magnetic dynamo in the interior of stars and the processes leading to stellar activity, remains among the outstanding unsolved problems of modern astrophysics. During star formation, magnetic fields are probably central to despinning the protostellar nebula and forming an accretion disk surrounding the protostellar object (thus influencing planetary formation as well). Magnetic fields may regulate angular momentum loss from protostars and young stellar objects and regulate despin during subsequent T-Tauri and main sequence phases. Magnetic fields also play a key role in transporting angular momentum in stellar interiors and are the most likely cause of virtual solid body rotation in the deep interior of our Sun. The formation of jets emanating from protostellar objects, the driving of stellar winds from late-type stars of all ages, and the creation and regulation of stellar activity are all strongly influenced by magnetic fields. We can study stellar magnetic fields and all associated processes through observations of the X-ray emitting plasma distributed over the surface of stars by stellar activity.

With Constellation-X we will extend the plasma diagnostic techniques so far applied only to our Sun (for measuring temperature, density, elemental abundances, and ionization equilibrium, e.g., Antonucci, 1989) to a large sample of stars. Such observations will invoke new structural diagnostics such as photospheric fluorescent Fe K lines (excited by coronal X-rays) and will couple these data with density diagnostics and rotational Doppler broadening. In addition to transitions in He-like and H-like charge states of abundant elements such as O, Ne, Mg, Si, S, Ar, Ca, and Fe, Constellation-X will observe dielectronic recombination satellite lines as well as transitions in the Fe L-shell complex. Detailed characterization of thermal plasma properties over the widest range of stellar parameters will address the detailed physics of how coronae are structured and heated as a function of spectral type and stellar activity levels, including pre-main sequence stars.

# 2 constellation-x

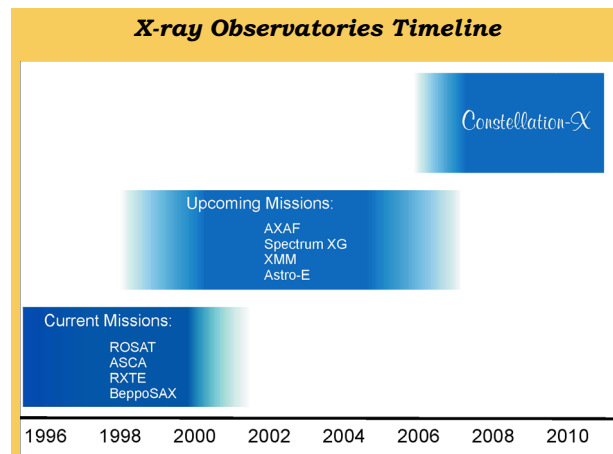
*High throughput, high resolution X-ray spectroscopy . . .*

## 2.1 X-ray Astronomy Comes of Age

In essentially all cases in which gravitational forces are important to the dynamics and energetics of a system, the presence of X-ray emitting gas is a natural consequence. As such, X-ray observations play a crucial role in addressing the origin, structure, and evolution of the Universe and of its principal material constituents: dark matter, clusters of galaxies, galaxies, stars, and planets. Viewing the X-ray sky presents unique technological challenges because X-rays cannot penetrate Earth's atmosphere. Space-based observatories are required and this has led to X-ray astronomy being one of the outstanding success stories of the space program. The first extra-solar X-ray source was discovered from a short rocket flight in 1962. As detector and telescope technology has matured, enormous progress has been made by a series of ever more capable missions. In 1978, the flight of the first sensitive X-ray focusing telescope on NASA's Einstein Observatory revealed that virtually every class of astronomical object emits X-rays. Since then, the EXOSAT, Ginga, ROSAT, and ASCA satellites have laid the foundation for X-ray astrophysics. All that we have learned during this time has brought us to the current phase of X-ray astrophysical studies, which will climax with the launch of the Chandra, XMM, and Astro-E missions. Surely these missions will bring discoveries and surprises; however, the results in hand from past X-ray astronomy missions, as well as from other wavebands, have already shown the way forward. A dedicated high resolution X-ray spectroscopy facility with sufficient collecting area to reach the faintest source populations seen in the ROSAT deep surveys (a factor of 10 deeper than the Einstein deep fields) is required for X-ray astronomy to come of age and become a true discipline of astrophysics.

X-ray spectroscopy is especially useful for investigating issues related to the origin and distribution of the elements. The soft and medium energy X-ray bands contain the K-shell lines for all of the abundant metals (carbon through zinc) and the L-shell lines of most. These are bright, allowed transitions with large equivalent widths. In general, all charge states are accessible. Hence the ability to measure elemental abundance is not strongly dependent on the physical state of the emitting gas. Studies in the X-ray band complement the infrared, optical, and ultraviolet bands, in which only certain molecular and/or ionic species can be measured for each element. The detailed X-ray line spectra are rich in

plasma diagnostics that can be used to provide unambiguous constraints on physical conditions in the source. To date these diagnostics have not been extensively exploited, primarily because the energy resolution of current detectors (CCDs) is not sufficient (Figure 2). In addition to the better energy resolution, a substantial increase in collecting area (throughput) is required to exploit these diagnostics.



With adequate near term funding, a 2007 launch is feasible. Around that time, Chandra will be reaching the end of its nominal mission lifetime. The multi-satellite production line approach provides an opportunity to add capability after the initial Constellation is launched. Possibilities include increasing collecting area and exploiting ongoing improvements in technology to give better angular/spectral resolution, field of view coverage, and bandpass.

## 2.2 Mission Implementation

### 2.2.1 Effective Area

The fundamental mission requirement is to acquire spectra of high statistical quality in an observing time of  $10^5$  s or less at the faintest flux levels found in the ROSAT deep surveys ( $2 \times 10^{-15}$  ergs  $\text{cm}^{-2}$   $\text{s}^{-1}$  in the 0.2 to 2.0 keV band). In addition, for many astronomical sources, short-term variations in the X-ray spectra provide a crucial key to the underlying physics. For stellar flares, the timescales of interest are of order tens of seconds, while for active galactic nuclei, they are several hours. Variability studies require both large collecting area and continuous coverage. These requirements dictate an effective area

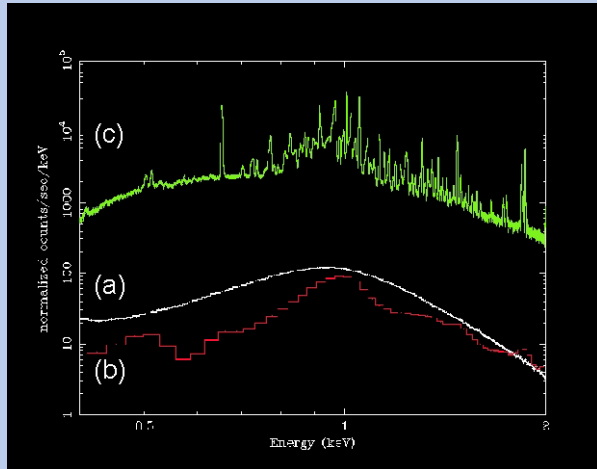


Figure 2. Simulations of a MEKAL plasma with a temperature of  $\sim 10^7$  K showing a comparison of the energy resolution of spectrometers used in X-ray astronomy. (a) The proportional counter, a detector commonly used in the early days of X-ray astronomy. This detector cannot resolve any distinct line features. (b) The CCD detectors on ASCA, Chandra, and XMM. With this resolution the hydrogen-like oxygen line at 0.65 keV and a helium-like silicon line at 1.8 keV can be distinguished from the broad iron L complex centered at 1 keV. (c) The grating spectrometer to be flown on XMM and Constellation-X. The exposure time for (c) is 10% of that for (a) and (b). With this resolution, the major line features can now easily be distinguished thus allowing detailed plasma diagnostics (see figures 5, 6, and 7).

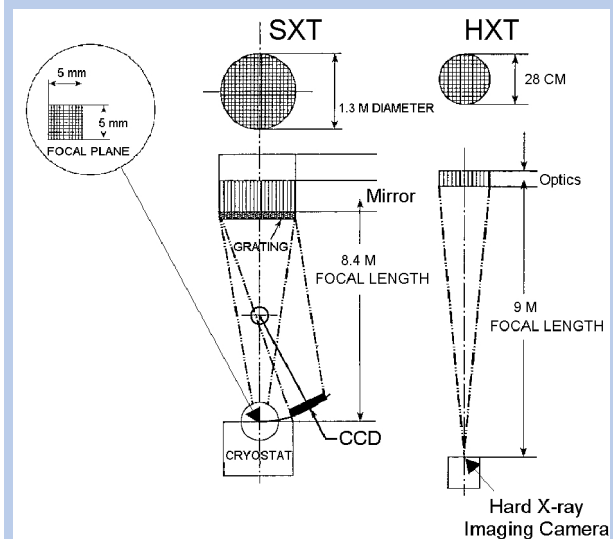


Figure 3. A schematic design of the instrument layout. Each “science unit” consists of a spectroscopy X-ray telescope (SXT) covering the 0.25 to 10 keV band and a hard X-ray telescope (HXT) covering from 6 to 40 keV. Behind the SXT mirror is a reflection grating array that disperses 50% of the beam to a CCD array. The remainder of the X-rays pass undisturbed to a micro-calorimeter array. For the HXT, X-ray optics are coated with multilayers to enhance their hard X-ray performance, to provide the first focusing capability in the hard X-ray band.

(including the spectrometer efficiency) of  $\sim 15,000 \text{ cm}^2$  at 1 keV,  $\sim 6,000 \text{ cm}^2$  at 6 keV, and  $\sim 1,500 \text{ cm}^2$  at 40 keV, resulting in a throughput 20 to 100 times higher than provided by the spectrometers on Chandra, XMM, or Astro-E.

The large collecting area is achieved with a design utilizing several mirror modules, each with its own spectrometer/detector system. The Constellation-X design recognizes that several spacecraft and more modest launch vehicles (e.g., Delta-class), each carrying one or a few science units, can cost less than one very large spacecraft and launcher (e.g., Titan-class). The program is robust in that risks are distributed over multiple launches and spacecraft with no single failure leading to a catastrophic loss of mission.

The prime objective of the Constellation-X mission is X-ray spectroscopy. We must first and foremost maximize the number of photons collected. X-ray telescopes typically use a grazing-incidence design and resemble long thin cylinders that are nested together. To maximize the collecting area per unit mass at minimal cost, we select an angular resolution that allows confusion-limited observations of the faintest source populations to be studied. This gives a requirement of  $\leq 15''$  half power diameter (HPD) below 10 keV and  $\leq 1'$  HPD above 10 keV. A  $10^5 \text{ s}$  exposure will obtain 1200 counts in the calorimeter at a flux of  $\sim 2 \times 10^{-15} \text{ ergs cm}^{-2} \text{ s}^{-1}$  (0.2 to 2 keV band). There are  $\sim 1000$  sources per square degree at this flux level. Because of the need for good signal to noise, these are the faintest sources likely to be observed with Constellation-X. Brighter sources will typically give tens of thousands of counts per spectrum.

Since it is not practical to cover the entire 0.25 to 40 keV band with a single telescope/instrument combination, Constellation-X will utilize two types of high throughput focusing telescope systems (Figure 3) to simultaneously cover the low (0.25 to 10 keV) and high energy (6 to 40 keV) bands (Figure 4). The low-energy Spectroscopy X-ray Telescope (SXT) is optimized to maintain a spectral resolving power of at least 300 across the 0.25 to 10 keV band pass. The high energy system (HXT), with lower spectral resolving power, overlaps the SXT and primarily is used to measure the relatively line-less continuum from 10 to 40 keV.

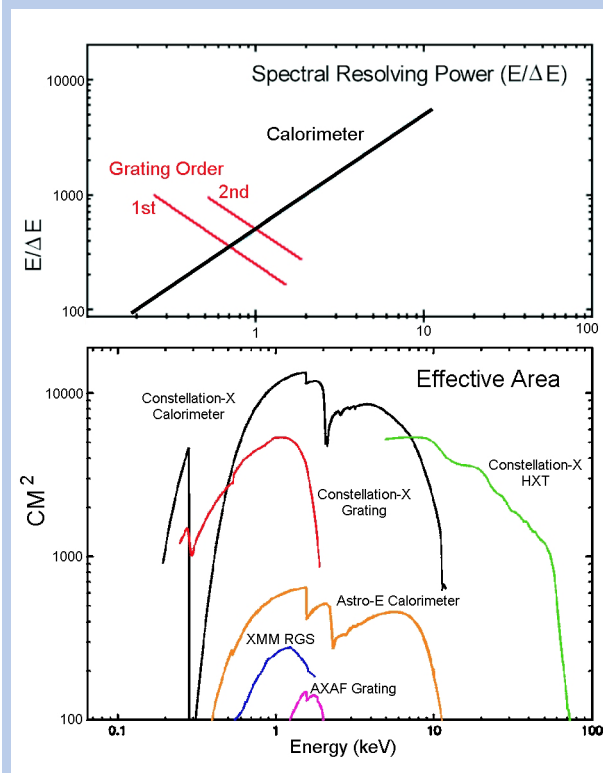


Figure 4. The lower panel shows the effective collecting area of the SXT and HXT systems, including the detector efficiency, with the grating and calorimeter curves shown separately. The effective area curves of the spectrometers with  $R > 300$  on Chandra, XMM, and Astro-E are also shown. Since the HXT is the first focusing optic to be flown in this band pass, there is no previously flown or planned comparison available. The resolving power of the SXT system is shown in the upper panel. Note that the resolving power of the non-dispersive calorimeter (fixed 2 eV resolution) increases with energy, whereas the resolving power of the dispersive grating spectrometer increases with decreasing energy, which makes the two systems complementary. The two systems are tuned to provide a minimum resolution of 300 at  $\sim 0.8$  keV.

lithium-like satellite lines from the overlapping helium-like transitions.

The SXT uses two spectrometer systems that operate simultaneously to achieve the desired energy resolution (Figure 3): (1) a 2 eV resolution quantum microcalorimeter array with a  $2.5'$  field of view, and (2) a set of reflection gratings for energies  $< 2$  keV. The gratings deflect part of the telescope beam away from the calorimeter array in a design similar to XMM except that the direct beam falls on a quantum calorimeter instead of on a CCD. The two spectrometers are complementary, with the grating optimal for high resolution spectroscopy at low energies and the calorimeter at high energies. The gratings also provide coverage in the 0.3–0.5 keV band where the calorimeter thermal and light-blocking filters cause a loss of response. This low-energy capability is particularly important for high-redshift objects, for which line-rich regions will be moved into this lower energy band.

Examples of the plasma diagnostic lines of some of the more abundant elements for the He-like transitions to be observed with Constellation-X are shown in Figure 5. These lines cover temperatures of 1 to 100 million degrees and

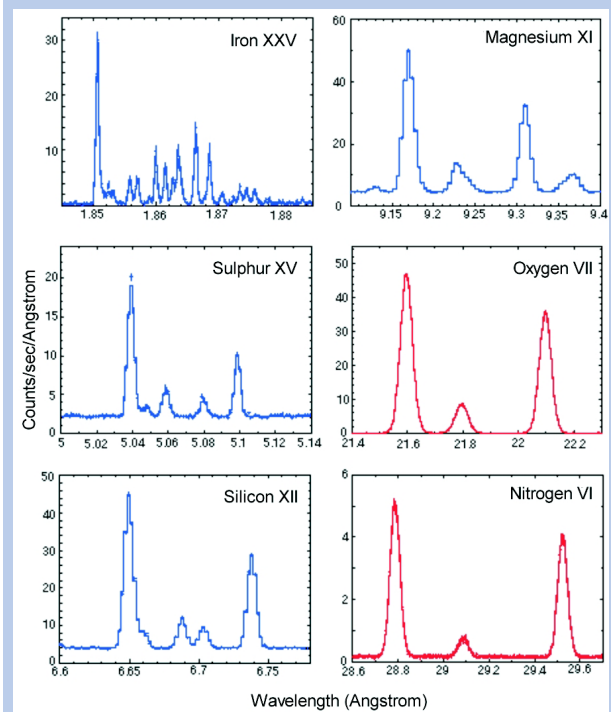


Figure 5. A Constellation-X simulation of an 80,000 s exposure of AR Lac illustrates key helium-like transitions that will be used to determine plasma density and temperature. Clearly resolved in all cases are the resonance, forbidden, and intercombination lines. The Fe XXV simulation utilizes the calorimeter while the others utilize the grating/CCD system.

### 2.2.2 Spectral Resolution

High spectral resolution is essential to make unique line identifications. The detailed X-ray line spectra are rich in plasma diagnostics that provide unambiguous constraints on physical conditions in celestial sources. A spectral resolving power of at least 300, for example, is required to separate the density-sensitive He-like triplet, while in the region near the iron K complex, a resolving power exceeding 2000 is necessary to distinguish the

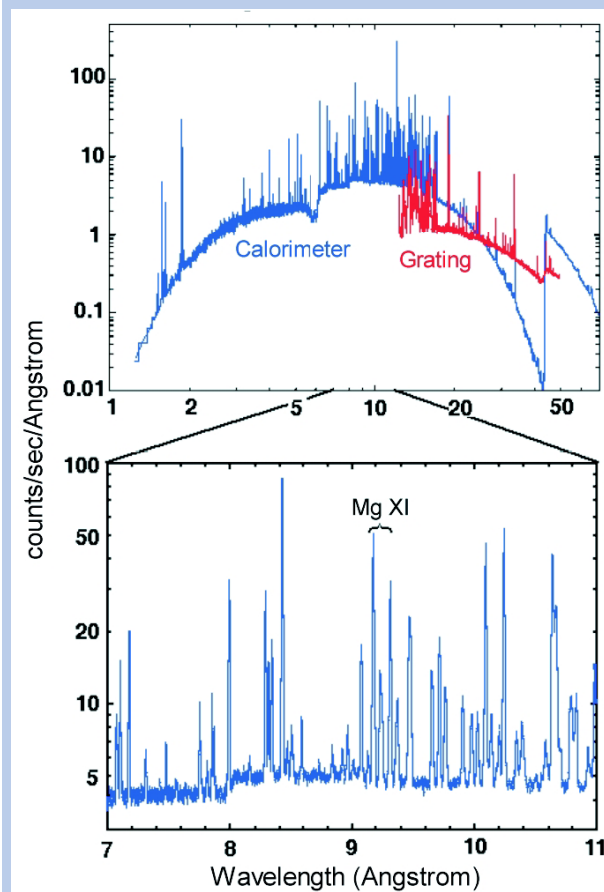


Figure 6. A simulated spectrum from an active stellar coronal system (an RS CVn) to illustrate the power of X-ray spectroscopy. The model consists of thermal plasma emission from gas with temperatures of 7 and 24 million K. A forest of lines is seen, the vast majority of which will be resolved. The lower panel shows a blow up of the part of the spectrum that contains the helium-like lines of magnesium. Note how the grating fills in the important region around 40Å.

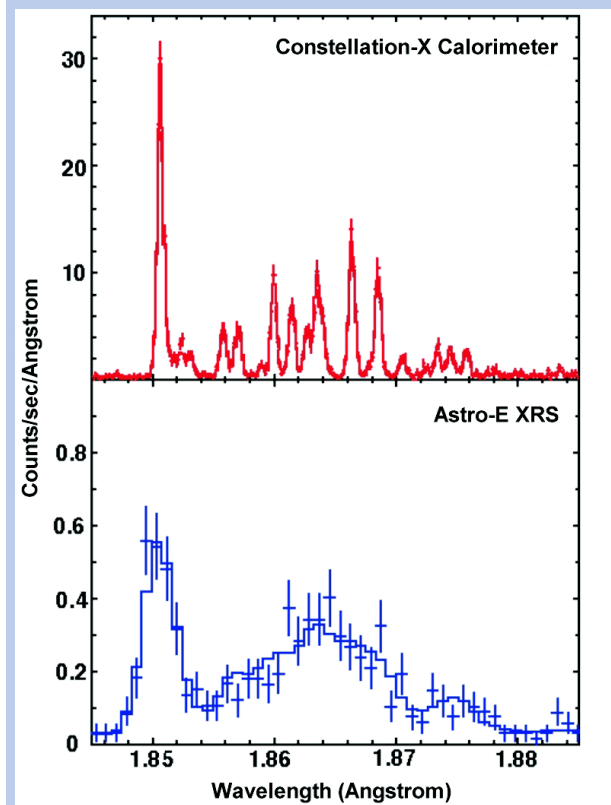


Figure 7. Simulations of helium-like iron (Fe XXV) emission from a ~20 million degree plasma. The top panel shows the spectrum from the Constellation-X calorimeter, which is currently under development. The bottom panel shows the spectrum from the microcalorimeter to be flown on Astro-E. The Astro-E calorimeter provides a major advance over current capabilities and will resolve the resonance line from its satellites for the first time. The Constellation-X calorimeter will resolve the entire satellite complex with a resolution similar to that currently used to observe the Sun. Note also the increased throughput of the Constellation-X system.

plasma densities of  $10^8$  to  $10^{14}$   $\text{cm}^{-3}$ . Figure 6 illustrates the power of the Constellation-X spectrometers with a simulated observation of an active stellar coronal source (the RS CVn star AR Lac). For simplicity, a two-temperature model of 7 and 24 million K (although a more continuous distribution of temperature is more likely to be found) is used to highlight the richness of the spectrum. The upper panel shows the spectrum as a function of wavelength with the portion centered on the He-like Mg line shown on an expanded scale in the lower panel. Notice that the grating covers the vital low-energy part of the spectrum, which includes the He-like transitions of over 20 elements.

To compare the spectral resolving power of the Constellation-X calorimeter with that of Astro-E, similar duration observations of a stellar corona are shown in Figure 7. The top panel shows the Constellation-X spectrum while the lower panel shows the Astro-E calorimeter spectrum. The crosses indicate the statistical uncertainties for the observed counts in each individual energy bin. Constellation-X fully resolves the satellite lines and obtains an order of magnitude more counts as well.

Measurement of accurate radial velocities from X-ray emission lines is central to many astrophysical investigations such as mapping the velocity fields of clusters of galaxies, obtaining flow velocities in stellar flares, mapping the

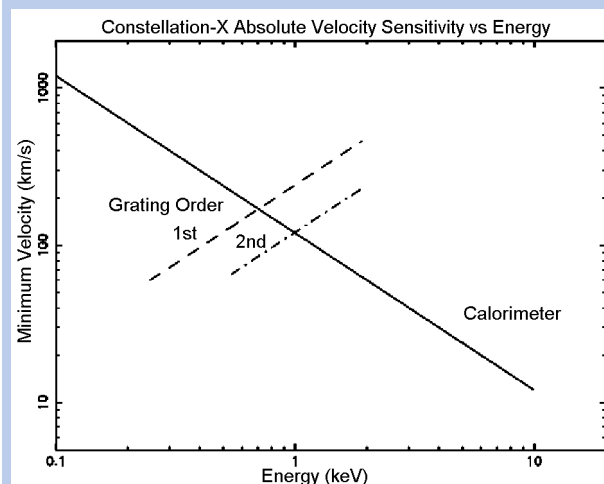


Figure 8. The sensitivity for using X-ray lines to measure absolute velocity as a function of energy. This assumes the absolute velocity can be measured to five times better than the detector resolution. Notice that for a calorimeter or any device with a fixed resolution (in this case 2 eV), the velocity sensitivity increases linearly with increasing energy. At 6 keV a calorimeter with 2 eV resolution gives an absolute sensitivity of order 20 km s<sup>-1</sup>. In contrast, for a dispersive grating spectrometer the velocity sensitivity scales in exactly the opposite sense, with the highest velocity sensitivity at low energies.

coronae of RS CVn and other binary systems, and measuring the kinematics of clumps of ejecta in supernova remnants. These require velocity sensitivity (the ability to centroid a line) better than 100 km s<sup>-1</sup> below 1 keV (see Figure 8). At the higher energy of the iron K line, the velocity sensitivity of order 20 km s<sup>-1</sup> achievable with Constellation-X will provide radial velocity measurements enabling us to determine the mass distribution of black holes, neutron stars, and white dwarfs for a large sample of binary systems.

Compared to other non-focusing methods such as those used for RXTE, Constellation-X has twice the area, 640 times the energy resolution, 240 times the spatial resolution, and, above 10 keV, 100 times the sensitivity. With individual pixels that can accept count rates of 1,000 counts/second, the combined count rate over the calorimeter arrays of four spacecraft, Constellation-X will be able to look at sources as bright as 10,000 counts/second (i.e., bright X-ray binaries) and thus is a more powerful follow-on to RXTE.

### 2.2.3 Bandpass

Many cosmic X-ray sources exhibit characteristic spectral features over a broad range of energy. These include (1) AGN, in which Compton reflection off surrounding cold material produces a “tail” to the continuum spectrum at energies > 10 keV, while fluorescence and recombination radiation from the same medium produces a range of discrete emission and absorption features down to low energies; (2) stellar flares, in which a hard, nonthermal, impulsive continuum can accompany the line-rich thermal emission produced by heating of coronal plasmas; and (3) supernova remnants, in which synchrotron radiation generated by cosmic ray electrons accelerated at the shock front can produce a hard extension to the thermal spectrum from shocked gas. Unambiguous measurement of such effects requires a bandpass which extends from ~ 0.2 keV to at least 40 keV. The Constellation-X hard X-ray telescope (HXT) uses

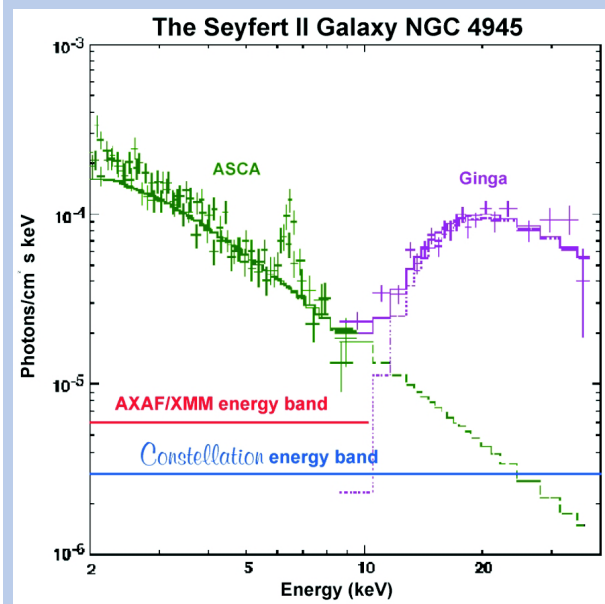


Figure 9. This combined ASCA and Ginga spectrum (the observations were not simultaneous) of the Seyfert II galaxy NGC 4945 illustrates the need for the hard X-ray telescope. The continuum source is heavily absorbed, probably by an optically-thick torus, and is only seen above 10 keV, exactly where telescopes like Chandra and XMM cut off. At lower energies, only emission scattered around the torus is seen. Constellation-X will for the first time be able to measure the underlying continuum and the scattering component simultaneously. This will enable the total energy output to be determined. By observing a large sample of such systems, the overall accretion geometry of AGN should be revealed. Observations will be possible for systems that are a factor of 100 times fainter than NGC 4945, thereby covering a wide range of luminosity and redshift.

multilayer coatings on individual mirror shells to provide the first focusing optics system to operate in the 6 to 40 keV band. No current or upcoming X-ray observatory provides similar high-energy sensitivity. Chandra and XMM, designated as the workhorses of X-ray astronomy in the next decade, will detect photons with energies only up to  $\sim 10$  keV.

Compelling motivation for the HXT is provided by the existence of sources whose energy output peaks in the 10–40 keV range. Figure 9 shows an example of such a source, the Seyfert 2 galaxy NGC 4945. The highly absorbed continuum X-ray emission from the AGN, which is obscured by an optically-thick torus, is visible only above 10 keV. For energies less than  $\sim 10$  keV, where Chandra, XMM, and Astro-E are sensitive, only the X-rays that are scattered around the torus are seen. Measuring the continuum above 10 keV is crucial for understanding the true nature of the source. With its hard X-ray sensitivity, the HXT can detect sources with column densities as high as  $10^{25}$  cm<sup>-2</sup>. For obscured AGN, which may make up the majority of the XRB, the HXT becomes background dominated at a flux of about  $10^{-14}$  ergs cm<sup>-2</sup> s<sup>-1</sup> (10–20 keV). In addition, about 55% of the 10–40 keV X-ray background is expected to come from sources with flux levels above  $10^{-14}$  ergs cm<sup>-2</sup> s<sup>-1</sup> and thus will be easily detectable for moderate HXT exposures. In summary, with the HXT, Constellation-X will be able to study AGN with the highest X-ray absorbing column densities and will go to much deeper flux levels, thus obtaining spectra for thousands of such objects.

# 3 Example Mission Science

*Studying the life cycles of matter in the Universe . . .*

## 3.1 Matter Under Extreme Gravity

Our confidence that active galactic nuclei are powered by the release of gravitational energy provides only a small step toward our understanding of how matter behaves under extreme gravity. From small to large scales, many important questions still abound. How does the accreting material make its way into the surroundings of the black hole? How is this material fed directly into the black hole? How do jets form? How do black holes participate in the formation and evolution of galaxies? Is the QSO phenomenon more common in the past than it is today? And if so, why?

Constellation-X is designed to answer these questions by probing the central power source of AGN while mapping the geometry of the surrounding material. The large collecting area will provide the first spectra at high resolution for lower luminosity and/or high redshift AGN populations at fluxes of  $\sim 10^{-14}$  ergs  $\text{cm}^{-2}$   $\text{s}^{-1}$ . For the brightest AGN, time-resolved, high resolution spectroscopy on timescales of minutes will be possible for the first time. The broad bandpass will allow a measurement of Compton reflection (where the spectrum from the central engine is modified by the effects of reprocessing in the surrounding material) and will permit detailed studies of highly-absorbed Seyfert II galaxies. The broadband capability will allow a determination of the high-energy cutoff in the continuum of intermediate to high redshift QSOs, since the spectral break predicted in the range 50–200 keV is redshifted into the Constellation-X band for  $z \sim 1$ –2. At lower energies, the band pass is optimal to measure the absorption from inflowing material, including time variable effects.

### 3.1.1 Supermassive Black Holes

#### Closing in on Black Holes

The intrinsic AGN spectrum is a featureless power law and hence conveys limited information about the geometry and physical state of matter in the vicinity of the black hole. On the other hand, some fraction of these X-rays illuminate the underlying disk of accreting matter, and the subsequent reprocessing imprints atomic features into the observed spectrum (Figure 10). When the hard X-ray continuum illuminates the disk, Compton scattering, photoelectric absorption, and fluorescent line emission all come into play and determine the spectrum that is scattered/re-emitted from the disk. The main effect of adding this “reflection” to the spectrum is to create a hardening above  $\sim 10$  keV and a  $K\alpha$  fluorescent emission line of iron at 6.4 keV.

The reflection features provide a powerful probe of the physics of the accretion flow, as well as the spacetime geometry close to the black hole. The Fe  $K\alpha$  emission line is particularly important because it acts like a clock in the immediate vicinity of the black hole with which we can probe the accretion disk motion (via the Doppler effect) and the strong gravitational field (via gravitational time dilation). Observations of bright nearby AGN with the ASCA satellite have already revealed the line to be extremely broad and asymmetric, as expected if it originates from the innermost regions of a black hole

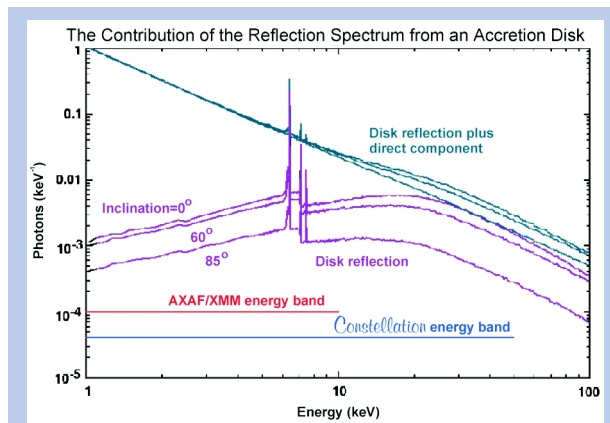


Figure 10. The reflected and composite X-ray spectra predicted for a flat, optically thick, non-rotating accretion disk illuminated by an isotropic source of primary X-rays located on-axis and above the center of the disk (Lightman and White, 1988; Guilbert and Rees, 1988). Reflection spectra for three different viewing inclinations are shown (George and Fabian 1991). Constellation-X will observe the reflected spectrum out to much higher energies with better sensitivity than other currently planned spectroscopy missions.

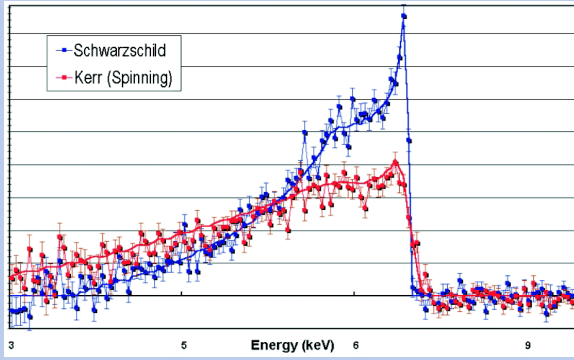


Figure 11. Constellation-X will allow detailed measurements of the Iron  $K\alpha$  emission line profile in AGN and will measure the gravitationally induced increase in photon wavelength as matter is pulled closer to the event horizon of the black hole. This simulation shows what Constellation-X might see for iron line profiles from accretion disks orbiting Schwarzschild (non-spinning) and Kerr (spinning) black holes.

accretion disk. Such observations provide the most direct evidence for the strong gravity associated with supermassive black holes at the hearts of AGN.

The broad lines exhibit characteristic signatures of general relativistic effects resulting from the enormously strong gravity within 10 Schwarzschild radii of the black hole. From the distortion of the line profile by these effects, it is possible to measure the mass and spin of the black hole and to test general relativity. However, these detailed tests are possible only with the increased collecting area, improved spectral resolution, and broad bandpass of Constellation-X to eliminate contributions from any narrow line components from material from much further out, to resolve individual bright spots contributing to the broad line emission, and to determine fully the underlying continuum (which is very important when studying broad line features).

Optical astronomers use variations in emission line profiles and the response of the line flux to changes in the continuum to determine the geometry and kinematics of

gas located light days to light weeks from the nucleus. Constellation-X will extend these observations to map out the immediate environment of the central black hole only light hours across by observing the emission from material just seconds to hours before it is pulled beyond the event horizon of the black hole.

When an X-ray emitting flare erupts, it takes a finite time for those hard X-rays to propagate to the disk and excite iron fluorescence. As the echo of the flare sweeps across the disk, the observed iron line profile and strength will change due to these finite light travel times. This is referred to as reverberation. Constellation-X will be able to follow the line variations due to large flares. This will allow the spatial distribution of flares, the ionization structure of the underlying accretion disk, and the mass of the black hole to be studied. Furthermore, there are robust reverberation signatures which differ for slowly and rapidly rotating black holes (Figure 11).

Figure 12 illustrates the concept of iron line reverberation. The time delay between the observed flare emission and the line response provides direct information on the mass of the black hole (current X-ray data, which only measure the

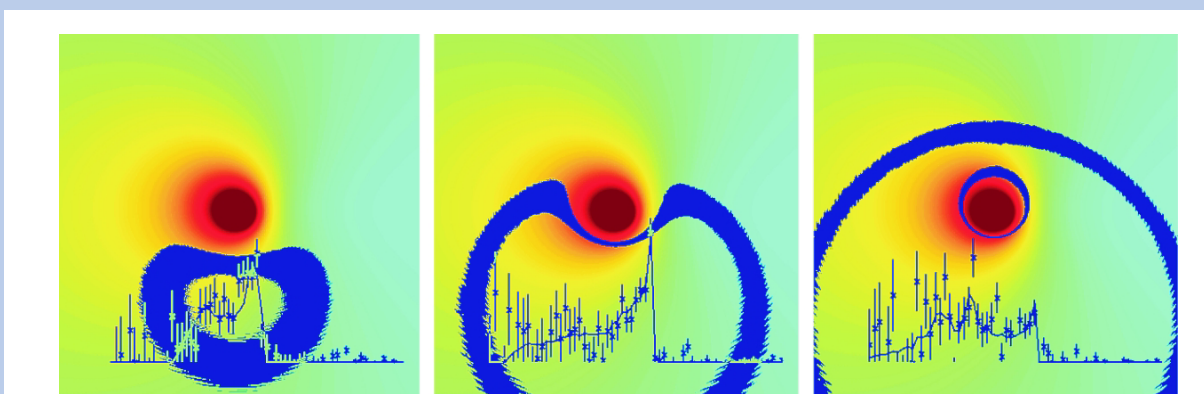


Figure 12. The ‘observed’ images of an accretion disk around a maximally-rotating  $10^8 M_{\odot}$  black hole, color coded to show regions of redshift and blueshift. The source has a time-averaged 2–10 keV flux of  $\sim 4 \times 10^{-11}$  ergs  $\text{cm}^{-2} \text{s}^{-1}$  (similar to, MCG–6-30-15) and the inclination of the disk is  $30^{\circ}$ . The figures illustrate the sequence of events after a large flare erupts on-axis at a height of 10 gravitational radii above the disk plane. The observed ‘echo’ of the flare is shown as a dark band for three given times (10000 s, 12000 s, and 14000 s) after the flare is observed directly. The corresponding iron line profiles are shown, together with data from 1000 s Constellation-X simulations (corresponding to the light crossing time of the black hole). Figures supplied by Chris Reynolds.

time-averaged line profile, cannot constrain the mass). Even more exciting is that for rapidly rotating holes, the fluorescing regions of the disk can extend down very close to the event horizon due to the stabilization of the disk orbits by the relativistic inertial frame dragging. In these cases, when a disk-flare erupts, a ring of line emission propagates outwards to large radii as expected, but another ring propagates inwards asymptotically approaching the event horizon. This appears as a distinct bump in the iron line profile that progressively moves to lower energies, providing a unique measure for black hole spin (a measurement only possible in X-rays).

## Geometry of the Accretion Flow in AGN

It has been established observationally that a significant amount of gas is present within the cores of AGN. X-rays illuminate the inflows and outflows around the nuclei in a manner that is rich in spectral diagnostics. Spectral signatures of this gas may include substantial absorption of the central continuum source and reprocessing features seen in emission. Approximately 50% of radio-quiet AGN show evidence for absorption by ionized matter along the line of sight (Reynolds, 1997), the so-called “warm absorbers.” These same objects often possess the hard X-ray signature of reflection from Compton-thick material. Still other AGN possess the spectral signatures of absorption and fluorescence in neutral gas. It is possible that gas in the centers of all radio-quiet AGN has a similar geometry but that what we see depends on our viewing angle. For example, the ionized scattering medium seen in edge-on Seyfert 2 galaxies from optical polarization studies may serve as the ionized absorbing medium in face-on Seyfert 1 galaxies.

We are confident that some of the matter in AGN comprises a central accretion disk, but the location and nature of the rest of the ionized and/or cold gas is not clear. For example, the ionized absorbing gas may be associated with the optical broad line region clouds, it may be part of an AGN-driven outflow, or it may exist as an X-ray heated wind from the surface of the accretion disk. One problem is that the absorption features are frequently too narrow for their properties to be measured with current instruments. Also, the timescales for variability of the individual absorption edges, which would indicate the location of the warm gas, are poorly determined. And it is possible that a significant amount of X-ray reprocessing does not occur in the disk at all but in dense clouds in the form of a more distant torus.

Presumably, any matter within the vicinity of the active galaxy nucleus has the chance to ultimately become part of the accretion flow, and so understanding the form of this matter and how it is transported to the center will undoubtedly yield valuable clues to the cycles of AGN activity. Ionized absorbers will leave their imprint not only by absorption edges, which are their usual trademarks in low resolution detectors, but also by absorption and emission lines. Such features can indicate the ionization state and velocity structure of the gas. On the other hand, the key to distinguishing between X-ray reprocessing in a central accretion disk and a more-distant torus lies in having the energy resolution necessary to separate narrow (low velocity) emission line components from broad (high-velocity) lines from a disk. In all cases, high sensitivity is required to monitor the spectral features on both long and short timescales.

For illustration, we examine two different cases of ionized absorbing media. One model includes turbulent motions

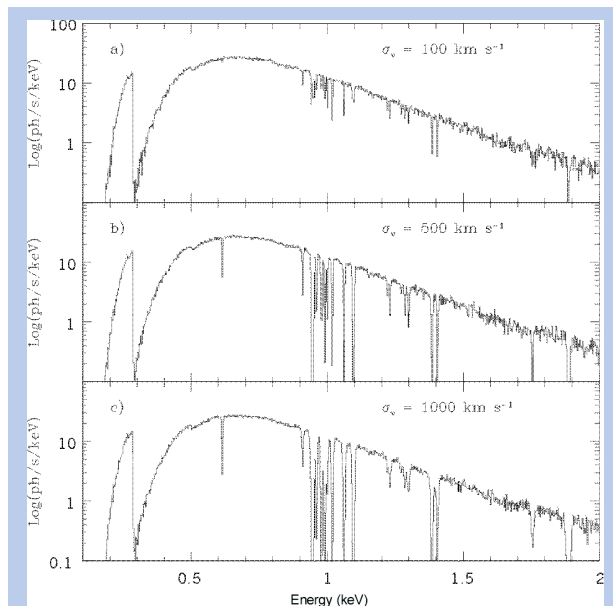


Figure 13. Constellation-X calorimeter simulations of a 20 ks exposure of the ultrasoft, narrow-line Seyfert 1 galaxy IRAS 13224-3809 (Nicastro et al., 1998), which is one of the most X-ray-variable Seyfert galaxies known (Boller et al., 1997). A cloud dispersion velocity for the ionized absorbing medium of  $\sigma_v = 100, 500,$  and  $1000 \text{ km s}^{-1}$  is assumed in a), b), and c), respectively. The cut-off at low energy is partly due to the inclusion of neutral absorption from the Galactic column along the line of sight ( $N_H = 4.8 \times 10^{20} \text{ cm}^{-2}$ ). Constellation-X will allow us to monitor changes in partial covering by the occulting structures in the accretion disk, and will allow the turbulent velocities in the absorbing medium to be measured. Simulations by Giorgio Matt and Fabrizio Nicastro.

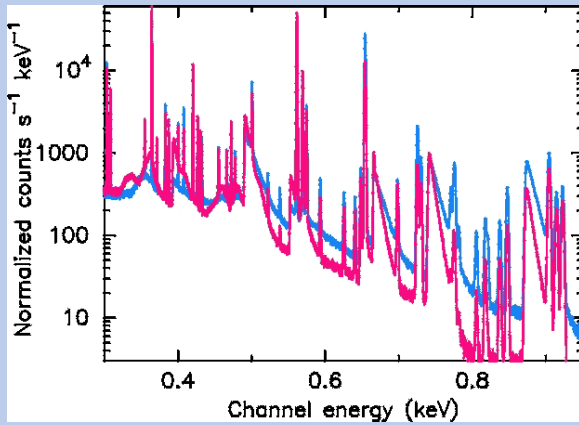


Figure 14. Simulated spectra for a 40 ks Constellation-X grating observation of an AGN with an absorber that is ionized, based on models from Hagai Netzer. The source flux is  $F(2\text{--}10 \text{ keV}) = 1 \times 10^{-11} \text{ ergs cm}^{-2} \text{ s}^{-1}$  and the continuum changes gradually from a power-law with  $\alpha = 2$  below 0.2 keV to  $\alpha = 0.9$  above 0.5 keV. The ionization parameters are  $U_X(0.1\text{--}10 \text{ keV}) = 0.15$  (bottom curve) and  $U_X(0.1\text{--}10 \text{ keV}) = 0.3$  (top curve). The absorber has  $N_H = 2 \times 10^{22} \text{ cm}^{-2}$ ,  $n = 1 \times 10^8 \text{ cm}^{-3}$  and solar metallicity, and the emission spectrum assumes the ionized material comprises a shell surrounding 80% of the illuminating

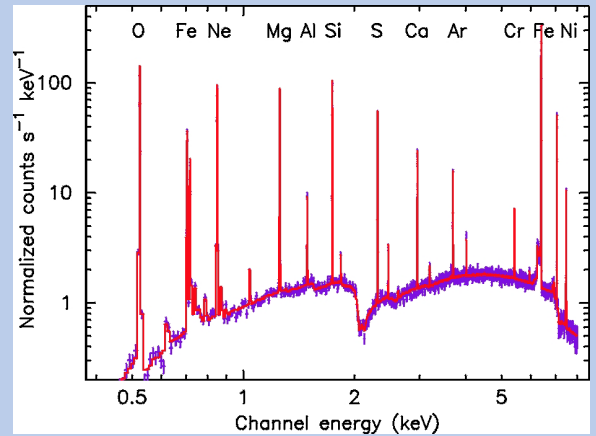


Figure 15. Simulated 20 ksec calorimeter observation of the Galactic center emission (reprocessed from an earlier epoch when the central AGN was much brighter). The emission is scattered in our direction by cold electrons in molecular clouds that are  $< 100 \text{ pc}$  from the galaxy center (Koyama et al., 1996). X-ray measurements such as this allow us to view the “fossil” of the continuum source as well as measure the composition of the gas at the center of our galaxy. Model supplied by Eugene Churazov.

of the gas and the other includes emission features. Many spectral features which would have been too narrow or weak to be detected by prior X-ray missions are predicted. The strength of absorption lines (Figure 13) depends on the turbulent motion of the matter, which broadens the line core. Turbulent velocities of hundreds or thousands of  $\text{km s}^{-1}$  would not be surprising since the optical emission lines in AGN have widths sometimes exceeding  $10000 \text{ km s}^{-1}$ . Multiple narrow emission features and recombination continua would also be detectable with the gratings (Figure 14).

Constellation-X will unravel the structure of line complexes such as Fe  $K\alpha$  by spectrally separating X-ray features that arise close to the black hole from those that arise far from the black hole. Intensive monitoring of bright AGN on all timescales will determine the fraction of the reprocessed emission from the disk compared to the regions further away. Such separation will finally allow us to derive meaningful physical parameters of the structure and geometry of the accretion flow in AGN. Constellation-X will also detect and resolve the wealth of weak absorption and emission features produced by the absorber. The absorption lines are intrinsically narrow, so broadening of the lines on the order of a few hundred  $\text{km s}^{-1}$  would indicate turbulent motions in the X-ray heated gas.

### The Galactic Center - A Dormant AGN?

Large amounts of obscuration (equivalent hydrogen column densities of  $10^{23}$  to  $10^{25} \text{ cm}^{-2}$ ) can significantly alter X-ray spectra by suppressing the continuum emission below 2–10 keV. Many nearby AGN such as NGC 4945 are heavily obscured and emit mostly at hard X-ray energies. What would happen, however, if the AGN were completely blocked, or if the black hole stops consuming fuel and the AGN activity turns off or drops into a radiatively inefficient mode? If a significant amount of gas remains near the center of such a galaxy, we would view the fossil signature of the AGN in the form of X-rays that have been scattered by the gas located some distance from the black hole. Since this light had to travel further to reach us, it is still visible even after the AGN engine has turned off. There appears to have been such a hidden source of X-rays at the center of our own Galaxy, which we see indirectly via scattered X-rays. The gas clouds that continue to fluoresce were exposed to the radiation from the central source long before the nuclear activity had turned off. Figure 15 shows a Constellation-X simulation of scattered X-rays from the still-illuminated clouds in the Galactic center. Similar spectra, with multiple emission lines, would be expected for absorbed AGN or variable AGN like NGC 4051 in its off state (which only lasts a few days).

## Heavily Absorbed AGN and the X-ray Background

We know that many nearby AGN are heavily obscured and emit mostly at high energies; however, could the same be true of more distant and powerful AGN? Interestingly, when added together, the integral X-ray spectrum of a large number of absorbed AGN at different redshifts with various column densities has a shape very similar to the hard X-ray background.

The energy density of the X-ray background peaks at  $\sim 30$  keV, but less than 15% of this total energy density can be accounted for by the ROSAT AGN population, which dominates the soft X-ray background. If AGN comprise the hard X-ray background, then most must have huge absorbing columns ( $N_H \sim 10^{22}-10^{25}$  cm $^{-2}$ ). Surveys by XMM, ABRIXAS, and Chandra, limited to energies less than  $\sim 10$  keV, will only probe absorbing columns up to a few times  $10^{23}$  cm $^{-2}$ . With its much higher sensitivity, the Constellation-X HXT can survey IR-selected AGN, probing faint and high-redshift AGN populations thus far inaccessible in the X-ray band. The data will also address questions about the geometry of the absorbing material.

## The High Redshift Universe

As we look toward the early Universe, we seek answers to basic questions of formation and evolution of structure on all scales. Because accretion power is so prevalent and X-rays result directly from the accretion process, studies in the X-ray band can make fundamental contributions. The Universe from  $z = 0$  to  $\sim 4$  is populated with a large variety of X-ray emitting AGN, such as radio galaxies, radio-quiet quasars, blazars, Seyfert galaxies, and LINERs. But are all these AGN really different, or do they merely reflect varying aspects of the same physical phenomenon? It seems likely that many of the differences, e.g., the radio-loud/radio-quiet dichotomy, are imprinted right at the heart of the central engine. Since iron lines and reflection features provide the best probe of this environment, they hold a vital key to understanding these fundamental class differences.

ASCA has shown that the brightest Seyfert galaxies have broad iron lines indicative of radiatively efficient, geometrically-thin accretion disks extending all the way down to the radius of marginal stability (i.e., the radius within which material rapidly spirals into the black hole). The other classes of AGN only have a very small number of objects bright enough to study currently. Even so, the results are fascinating. Strong broad lines are often weak or absent in luminous objects (Figure 16) and radio-loud objects. Ionization of the accretion disk, disruption of the inner cold disk into an advective state, or dominance of a beamed jet component are all possible explanations for these trends.

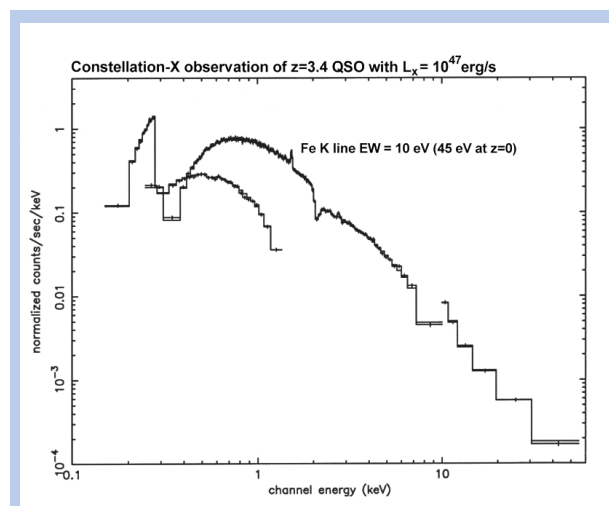


Figure 16. Constellation-X grating, calorimeter, and HXT simulation of a quasar at  $z = 3.4$  with an X-ray luminosity of  $10^{47}$  ergs  $s^{-1}$ . The Fe  $K\alpha$  line, which is 10 eV equivalent width in the observed frame, is predicted to be weak for this high luminosity object (Nandra et al., 1997) but easily detected.

With the throughput of Constellation-X, broad iron lines and reflection continua can be studied in thousands of AGN over a large range of  $z$  (Figure 17). With so many members open to study, the nature of the accreting material for any given class of AGN will be firmly established. We will have the data with which to answer questions that have only previously been in the realm of the theorists. Does jet production in radio-loud objects require a hot accretion disk? Are rapidly rotating black holes also required? Do X-rays from a beamed jet swamp a Seyfert-like reflection component in radio-loud objects? Are jets always perpendicular to the plane of the inner accretion disk? Do accretion disks become more highly ionized as one considers more luminous objects? Are low-luminosity AGN accreting in an advection dominated mode, and at what accretion rate does an advection dominated mode occur? These fundamental questions of AGN research can be best answered by probing the central engine directly via X-ray reflection studies.

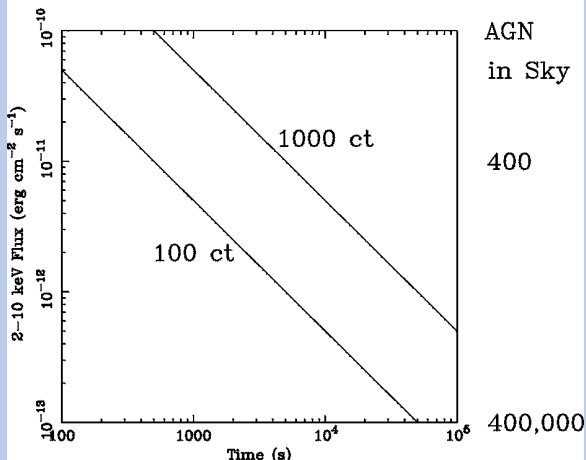


Figure 17. Predicted number of iron line photons collected by Constellation-X as a function of source flux and integration time. Also shown are the number of AGN on the sky at given flux levels. Note that  $\sim 1000$  iron line photons are required to define an accurate line profile. In a typical exposure time of  $10^4$  s, there are  $\sim 1,000$  AGN available for this study. Figure provided by Chris Reynolds and Andy Fabian.

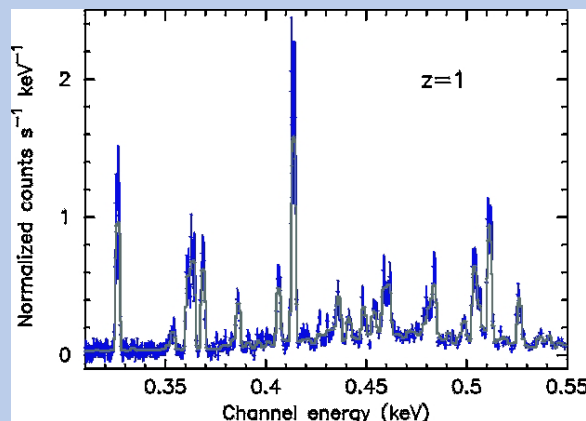


Figure 18. A simulated 100 ks Constellation-X grating spectrum of a heavily obscured and starbursting Seyfert galaxy at a redshift of  $z = 1$ . The X-ray properties of the starburst are similar to those of nearby starbursts but with a 0.2–2.0 keV luminosity of  $\sim 10^{44}$  ergs  $s^{-1}$ . The spectrum is modeled with a two-temperature thermal plasma having  $kT = 0.4$  and 0.9 keV and solar abundances. The AGN, with an intrinsic luminosity of  $\sim 6 \times 10^{44}$  ergs  $s^{-1}$ , is completely hidden at energies  $< 10$  keV by gas with a column density of  $N_H = 10^{24}$   $cm^{-2}$ , but the scattered (power-law) emission from the AGN contributes about 40% of the total flux between 0.2 and 2 keV. The Fe L emission line complex near 0.5 keV is a prime diagnostic of the physical properties of starburst-driven winds. These winds cannot be seen in the optical-UV band because of their very high temperatures. Constellation-X will allow reliable abundance determinations as a function of redshift for a large number of starbursting galaxies.

High- $z$  observations can be used to study galaxy evolution, star-formation, and the starburst-AGN connection. Optical studies indicate that the star formation rate in galaxies peaked at around  $z = 2$ . It has also been shown that the X-ray luminosity of the starburst correlates with  $L_{IR}$ , which increases with redshift and star-formation rate (David, Jones, and Forman, 1992). Local starbursts, like M82, have X-ray luminosities of about  $10^{40}$  ergs  $s^{-1}$ . If the X-ray luminosity scales with star-formation rate, then Constellation-X will observe thermal emission from starburst-driven winds out to redshifts of  $\sim 2$  (with  $L_x \sim 10^{43}$ – $10^{44}$  ergs  $s^{-1}$ ), i.e., during the epoch of peak star-forming activity. This is important because much of the energy of the starburst is contained in galactic-scale outflows, which have a plasma nature and are not visible in optical light. By studying the chemical composition of these winds for a large range in  $z$ , it will be possible to trace the evolution of the enrichment of the IGM (see also Section 3.2.2).

### 3.1.2 Stellar Endpoints

#### X-ray Binaries and Stellar Winds

##### *Stellar Black Hole Masses*

The velocity sensitivity of Constellation-X (Figure 8) will allow radial velocity measurements to constrain the mass function of X-ray binaries from X-ray observations alone. Optical studies have identified the best black hole candidates, including Cyg X-1, LMC X-3, and eight X-ray novae (e.g., A0620-00 and V404 Cyg; McClintock, 1998). In combination with X-ray pulse timing data, optical studies have yielded mass measurements for six neutron stars (e.g., Vela X-1 and Her X-1). Unfortunately, optical radial velocities can be measured for at most about 20% of X-ray binaries; in most systems, the optical extinction is too high or the effects of X-ray heating are too great.

In many X-ray binaries, a few percent of the X-rays emitted by the compact source will be intercepted by the atmosphere of the companion star. The most prominent feature in the reflected spectrum will be an Fe  $K\alpha$  fluorescence

line. This line is composed of the  $K\alpha_1$  and  $K\alpha_2$  components that have natural widths of 3.5 eV and a separation of 13 eV (Basko, 1978). These components will be further broadened by the rotation of the companion star (e.g., for  $v \sin i = 200 \text{ km s}^{-1}$ , the rotational broadening is 4.3 eV FWHM). Thus the  $\sim 2 \text{ eV}$  resolution of the Constellation-X calorimeter will resolve the individual  $K\alpha_1$  and  $K\alpha_2$  components and make it possible to track the radial velocities of a companion star in the same way that stellar velocities are tracked using optical spectra. Given the expected strength of the Fe  $K\alpha$  line, many X-ray binaries should be within the reach of Constellation-X. The unscattered core of the Fe  $K\alpha$  line should be the most easily detected feature in the reflected X-ray spectrum of the companion star.

Using the Fe- $K\alpha$  line, we can aspire to obtain firm dynamical data for all X-ray binaries even if a system lacks an optical counterpart. Some black hole candidates of great interest for which observations of the Fe- $K\alpha$  line may yield definitive dynamical data include the microquasars GRS 1915+105 and 1E1740.7-2942 and the 600-day transient 4U1630-47. For these systems, conventional optical/IR spectroscopy cannot or has not yielded any firm dynamical results. As an example of the Doppler modulation one might expect to see with Constellation-X, consider the eight black-hole X-ray novae which have an average full velocity amplitude of  $690 \text{ km s}^{-1}$  (McClintock, 1998). This corresponds to a full modulation of 14.7 eV (at Fe  $K\alpha$ ) or more than seven times the instrumental resolution of the calorimeter.

### *Stellar Winds*

Replenishment of the ISM, evolution of high-mass stars, evolution of X-ray binaries, and the powering of bright X-ray sources are all subjects that can be addressed by studying mass loss from stars in high mass X-ray binaries. Mass-loss rates and wind dynamics are currently most commonly studied in the UV and require complex models involving radiation transfer. Moreover, because of the limited bandpass available from UV spectrometers, there are limited diagnostics from which to extract reliable information. For X-ray bright neutron stars, we can use X-ray spectroscopy to infer mass loss rates from hot stars in high mass X-ray binaries. X-ray spectroscopy is uniquely powerful in that virtually all charge states of several elements can be observed contemporaneously. From the atmosphere of the companion, to the wind acceleration zone, to the magnetosphere of the neutron star, photoionization produces just such spectra. The ASCA spectrum of Vela X-1 reveals near-neutral fluorescence in Mg, Si, S, Ar, Ca, and Fe (Nagase et al., 1994). Lines appear as single blobs with ASCA, but it seems likely they are composed of a blend of low charge states throughout the X-ray illuminated wind. Constellation-X simulations of the spectrum in the Si K region (Figure 19) show that we will easily resolve different charge states. The velocity sensitivity of Constellation-X will enable a three-dimensional mapping of the spatial ionization distribution in the wind.

### *Cataclysmic Variables*

The unprecedented combination of energy resolution and sensitivity provided by Constellation-X will permit us to study subtle but potentially very useful line effects. One example involves recombination iron lines in situations in which opacity effects are important, as for instance in the standing shock above the white dwarf surface in Magnetic Cataclysmic Variables, which is believed to be responsible for their hard X-ray emission. The matter there is likely to

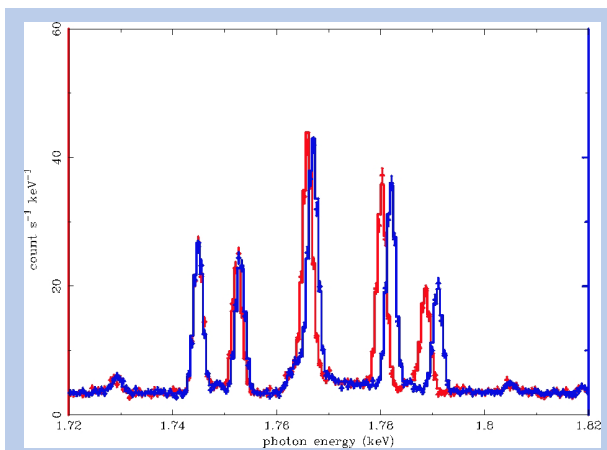


Figure 19. A small part of the spectrum of Vela X-1 around the Si K line complex as observed by Constellation-X in 10,000 s. This simulation represents one possible scenario for line formation in a high-mass X-ray binary and is based on the strength of the line seen by ASCA, assuming the line is made up of several charge states. The lighter curve represents lines formed in a stationary atmosphere. The darker curve represents lines formed in an accelerating stellar wind. Because of the ionization by the X-ray source, fluorescent K lines might be dominated by Doppler shifts rather than by Doppler broadening. The Si K emission line region is accelerating away from the observer and the velocity profile is such that the velocity/ionization relationship is linear with velocities of 100, 200, 300, and 400  $\text{km s}^{-1}$  for Si II, III, IV, and V, respectively. The maximum velocity comes from IUE observations of Vela X-1. The redshifts, allowing for the velocity projection, are 0.6, 1.2, 1.8, and 2.4 eV, respectively. Note that the Mg XII Ly beta line near 1.74 keV is not shifted. Figure supplied by Duane Liedahl.

be optically thin to photoelectric absorption and Compton scattering but thick in the center of the most intense lines. Figure 20 shows simulated Constellation-X calorimeter observations of the profiles of the Fe XXVI doublet for different column densities of matter. While for low column densities the matter is still thin in the line center and the line shape is still a Voigt profile (dominated by the Doppler core, from which the matter temperature can be derived), for larger densities the matter becomes thick in the line centers and a double horned shape is apparent, thus providing a probe of the geometrical and physical conditions of the emitting matter.

### Extragalactic Populations

X-ray binaries dominate the X-ray output of galaxies without an active nucleus (Figure 21). By studying them in other galaxies, we can see how their properties depend on the nature of the underlying galaxy. They also are all at a known distance and can be used as standard candles, e.g., using X-ray bursts to determine distance—or, given that we know the distance, testing whether X-ray bursts in fact provide a standard candle. Some of the most important results will undoubtedly come from obtaining stellar black hole mass estimates in nearby galaxies (from velocity diagnostics). For a typical luminosity of  $10^{38}$  ergs  $s^{-1}$ , Constellation-X will be able to study X-ray binaries in other galaxies out to a distance of  $\sim 10$  Mpc. These

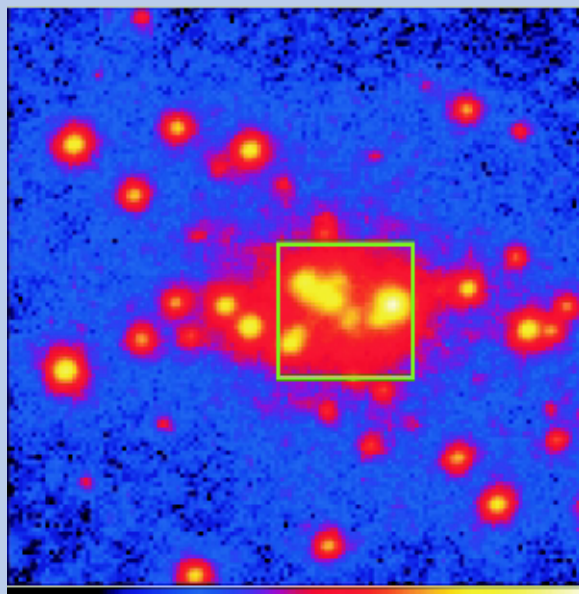


Figure 21. A simulated Constellation-X image of the nearby galaxy M31. The box shows the field of view of the calorimeter. The spectrometers will obtain high quality spectra for the sources visible in this image and will provide a data quality similar to that expected to be obtained for X-ray binaries within our own Galaxy by AXAF, XMM, and Astro-E.

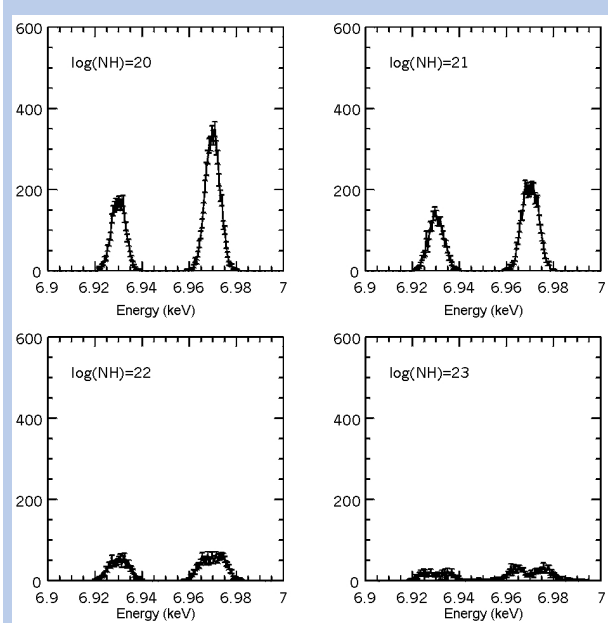


Figure 20. In Magnetic Cataclysmic Variables the accretion flow from the companion to the white dwarf surface is diverted by the magnetic field of the white dwarf. An accretion column with a hot shock front forms where the material is funneled. Many diagnostic line features are expected as the white dwarf surface and accretion stream is illuminated by the X-ray emission from the shock. Line emission will also be seen from the shocked region itself. This figure illustrates a 30 ks observation of a magnetic cataclysmic variable with the Constellation-X calorimeter. The Fe XXVI doublet is shown for a range of possible column densities through the shocked region. As can be seen the line intensity and shape are critically dependent on the column density through the accretion flow. Figure courtesy of Giorgio Matt.

observations will yield count rates from high resolution spectroscopy that are 10 to 100 times higher than from missions preceding Constellation-X. For objects in nearby galaxies such as M31 (Figure 21), we will obtain similar quality spectra to those for X-ray binaries in our own Galaxy (Figure 22).

### Isolated Neutron Stars

Neutron stars contain matter at densities, temperatures, and pressures that we cannot reproduce in laboratories on Earth. Such conditions were also present at early stages of the Big Bang. Thus neutron stars are a perfect astrophysical laboratory for astronomers to study physics at these extremes. Neutron stars are well known to astronomers as radio pulsars and many neutron stars have been detected in X-rays. The X-rays come from the stars' surface layers which can be heated by accretion or by heat

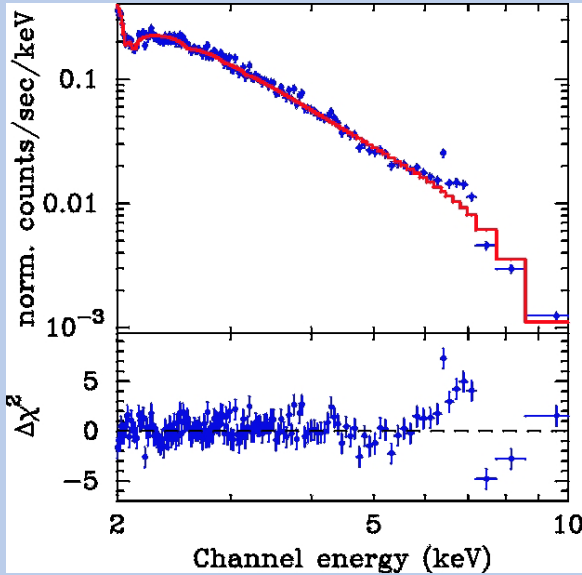


Figure 22. 40 ks simulation of a Circinus X-1 like X-ray binary located in another galaxy at a distance of 0.8 Mpc. The solid line is a two-component blackbody model folded through the instrument response. The narrow feature at 6.4 keV is the Fe K line. The broad feature is due to the strong 7.1 keV edge from the absorbing medium that partially covers the continuum source. Much can be learned from studying the variations in strength of the absorption over time. Figure supplied by Niel Brandt.

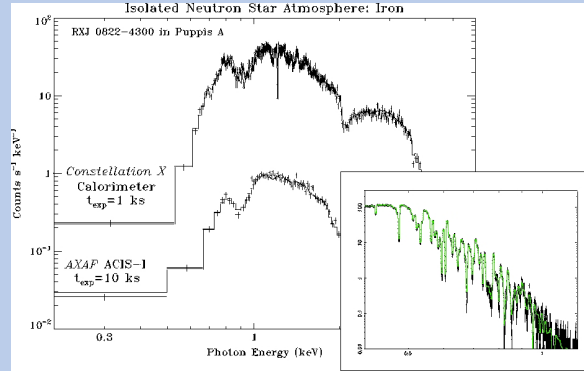


Figure 23. Simulated spectra of the atmosphere of the isolated neutron star RXJ 0822-4300 in Puppis A (main panel). The model is based on that of Zavlin et al. (1996) and includes the amount of iron expected for the case of solar abundances. The top curve represents a 1 ks Constellation-X calorimeter observation and the bottom curve represents a 10 ks Chandra ACIS-I observation. A narrow absorption feature due to iron is easily detected with the calorimeter. Inset: A 100 ks Constellation-X calorimeter simulation of a theoretical spectrum of the isolated neutron star RXJ0720.4-3125. In this case the neutron star is assumed to have a magnetic atmosphere (Rajagopal, Romani, & Miller, 1997). The absorption lines have widths of a few tens of eV and equivalent widths of a few eV. Figures supplied by George Pavlov and Slava Zavlin (main panel) and Tod Strohmayer (inset).

transported from the very hot stellar interiors. In studying neutron stars, we would like to understand their composition and physical properties of their superdense interiors. Although we cannot look directly inside these stars, studying their atmospheres can tell us much about their structure, their stellar ancestors, their environment, and their evolution. Once we understand the physical conditions of the neutron star surface layer, such as magnetic field, temperature, density, and chemical composition, we can infer its internal properties as well.

The thermal evolution of a neutron star depends on its internal composition, equation of state, and nucleon superfluidity. One of the most direct ways to determine the equation of state of neutron star matter is to determine the stellar mass and radius from measurements of bolometric flux and effective temperature. This is done by comparing the observed X-ray spectrum with reliable theoretical models. The neutron star evolution and the properties of its radiation strongly depend on the presence or absence of accretion, at present or at some past time. The primary effect of accretion is to change the chemical composition of the atmosphere, which can be determined from X-ray spectra. X-ray transients in quiescence may be isolated neutron stars accreting at a very low level (from the interstellar medium). Their spectra may be contrasted to the spectra of sources accreting at a high rate (from a companion), which should show approximately solar composition (from the transferred material). Understanding the chemical composition is important to finding how neutron stars interact with their environment, both at a very young age, when a fraction of the supernova ejecta can fall back on the star's surface, and over the whole life of the neutron star, which may include accretion episodes.

With its high sensitivity and spectral resolution, Constellation-X will enable investigations of neutron star atmospheres via X-ray continuum radiation and spectral lines. The most sensitive diagnostic of the surface gravity is the magnitude of the gravitational redshift of spectral lines, proportional to the mass-to-radius ratio. In addition, the overall shape of the X-ray spectrum depends on the surface gravity. Finally, pressure broadening of spectral lines provides a useful density diagnostic and serves as an indicator of the surface gravity. Combining these effects, we will be able to measure neutron star masses and radii and thus constrain the equation of state of superdense matter. The high resolving power of

Constellation-X will allow us to detect faint lines (with equivalent widths of only a few eV), measure low abundances, and make mass and radius determinations. Finally, the analysis of atomic spectral lines will provide the first direct measurements of magnetic fields of isolated neutron stars. Typical magnetic fields of these objects are expected to be so high that the structure of atoms and the resulting atomic spectra will be quite different of those in low magnetic fields. The magnetic fields can be measured by comparing the observed positions and strengths of spectral lines with their theoretical values calculated for a broad range of magnetic fields.

## 3.2 Life Cycles of Matter in the Evolving Universe

Constellation-X will address many questions related to the formation and evolution of clusters of galaxies and their constituents and the exchange of matter between them. In what follows, we give samples of the type of questions related to the structure and evolution of the Universe that can be uniquely answered with this mission. We begin with the largest structures and work our way down in scale.

### 3.2.1 Galaxy Clusters and the Intracluster Medium

#### Clusters of Galaxies

One of the most significant contributions of Constellation-X to the study of clusters of galaxies will be an accurate measurement of elemental abundances out to large distances. These measurements yield information about the metals produced by member galaxies over cosmic time. Constellation-X will determine or constrain for the first time the abundance of all elements with atomic number between those of carbon and zinc in clusters of galaxies. In particular, the evolution of the abundances of Si and Fe can be measured to  $z \sim 2$  for massive clusters and that of many other elements to  $z \sim 1$ .

Figure 24 shows a 50 ks Constellation-X observation of a typical cluster with a characteristic X-ray luminosity of  $3.5 \times 10^{44}$  ergs  $s^{-1}$ . The abundances are determined to 10% accuracy for Si, S, and Fe, and to 20% accuracy for Ne and Mg. This type of cluster has not been found in X-ray surveys to date because its flux of  $4 \times 10^{-14}$  ergs  $cm^{-2} s^{-1}$  is near the detection limit for extended sources of current instruments. Constellation-X observations of similar high redshift clusters (to be found by Chandra and XMM) will allow, for the first time, the overall abundance patterns and their dependence on redshift to be derived. These data will allow a direct comparison with the abundances of the damped Lyman- $\alpha$  systems, which are thought to represent the halos of galaxies, as well as with those of the Lyman- $\alpha$  forest. Constellation-X can determine the metallicity of the cluster gas to a higher redshift than optical and UV observations can measure the metallicity of normal galaxies.

Furthermore, the hard X-ray capability of Constellation-X will enable us to measure the elusive inverse Compton scattering radiation predicted in clusters of galaxies. Combined with radio measurements, the hard X-ray observations will yield a lower limit on the intracluster magnetic fields independent of equipartition or equal energy hypotheses. Detection of the nonthermal emission in clusters of galaxies has significant impacts on the underlying cosmological models through the estimation of the cosmological parameter  $\Omega$ . It also affects cooling flow arguments since the presence of the magnetic field can suppress the conduction of the cooling gas. Many clusters are believed to have formed through merger events as predicted in hierarchical large-scale structure models. As a result, due to the collision of subclumps and merging effects, shocks of very high temperature can be produced

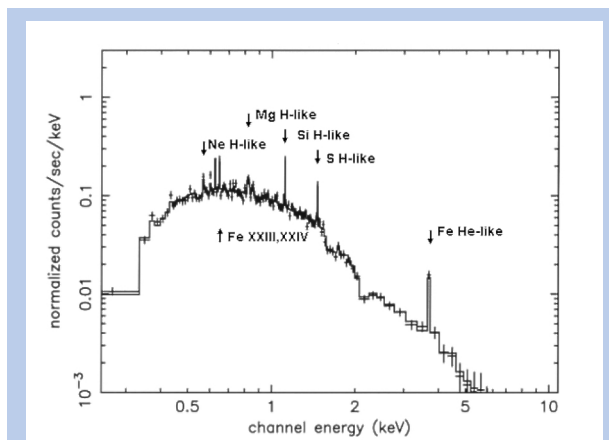


Figure 24. A simulated 50 ks observation of a cluster of galaxies with an X-ray temperature of 4 keV at  $z = 0.8$ . A Type II supernova abundance distribution was assumed. The abundances are determined to 10% accuracy for Si, S, and Fe and to 20% accuracy for Ne and Mg.

in the ICM. The hard X-ray observations will also shed light on the nature of clusters that show evidence of extremely high temperatures.

### Cluster Cooling Flows

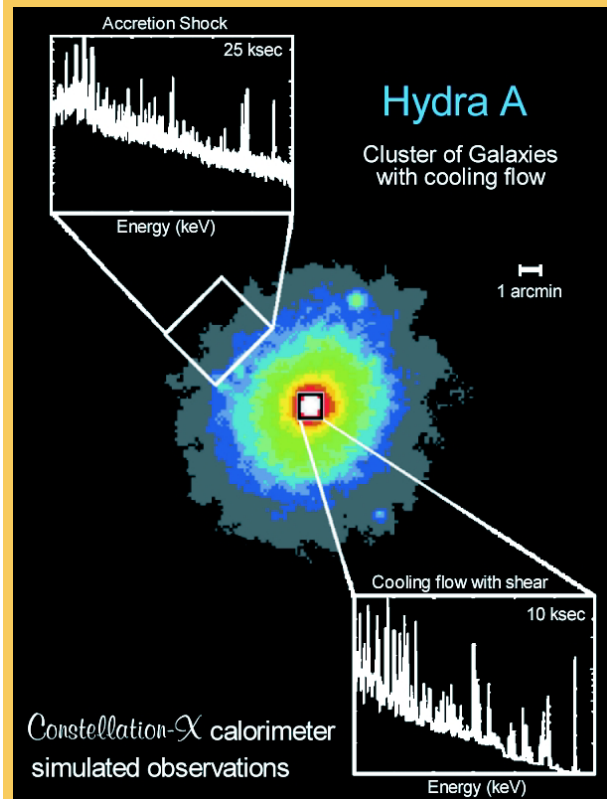
Constellation-X will also measure for the first time the mass motion of gas in the central cooling flow region of a cluster and in the “interaction region” of a merger candidate. This is important because a major discovery in recent years has been that most clusters are dynamical entities far from the static, spherically symmetric objects in hydrostatic equilibrium that they were once thought to be. ROSAT and Einstein observations have revealed that of all nearby clusters show strong evidence for interactions. Numerical simulations indicate that in a merger the gas velocities can range from 300–2000 km s<sup>-1</sup>. Such motions make determination of the total mass of such a system from X-ray temperature profiles uncertain without direct measurement of the velocity field. Constellation-X can easily detect relative velocities of 20 and 100 km s<sup>-1</sup> using the shift of the H-like Fe and O lines, respectively, and turbulence and mass motions of 200 km s<sup>-1</sup> via measurements of the width of these lines. For the first time, direct measurement of gas motion in clusters will be possible, thereby determining cluster merger parameters and strongly constraining models of cluster evolution. Optical spectroscopy of cooling flow clusters often shows gas with a velocity spread of up to km s<sup>-1</sup> located at the very center of the cluster (i.e., the inner ~ 10 kpc). Constellation-X will provide cluster-wide velocity information for many clusters while at the same time deriving the distribution of emission measure with temperature. These observations are crucial for understanding cooling flows, particularly the fate of the inflowing gas.

### Star Formation History in the Universe

In the hierarchical clustering picture, the star formation history of the Universe is determined both by the merging history of dark matter galaxy halos and by the complex astrophysical processes occurring within the baryonic material contained in these halos. While the former depends on cosmological parameters and the primordial fluctuation spectrum, the latter is sensitive to poorly understood aspects of star formation, such as the factors that determine the initial mass function (IMF) and the role of feedback.

Observationally, various optical/UV techniques have been used to derive estimates of the star formation rate (SFR) out to high redshift. Figure 25 shows optical and UV estimates of the SFR (filled circles) as well as the SCUBA submillimeter measurement (open circle; Hughes et al., 1998, and references therein). Star formation has been transformed to metal production using standard yields and IMF. UV/optical estimates must be considered as lower limits since these measurements are insensitive to star formation occurring in heavily dust-enshrouded environments; and in fact the SCUBA determination indicates that the star formation rate at  $z = 3$  may have been underestimated by a factor of five.

The deep potential well of galaxy clusters means that the ICM is a closed box for chemical evolution, with the amount of metals providing a fossil record of past metal production and, therefore, star formation. Figure 26 shows the



Constellation-X simulation of the spectrum of the Hydra A cluster of galaxies: the spectrum from the inner arcminute shows the simulated emission from the 300 M<sub>⊙</sub> per year cooling flow in Hydra A, and is characterized by multiple temperatures and a “shear” in the sense that the cooler gas has a larger velocity. The spectrum for the outer region shows emission from an accretion shock. Line emission from cool pre-shock gas can be seen superimposed on continuum emission from the hot post-shock gas. Such a shock, occurring at 1–3 Mpc from the center of the cluster, is predicted by numerical simulations but has not previously been observed because of the low X-ray surface brightness at large radii.

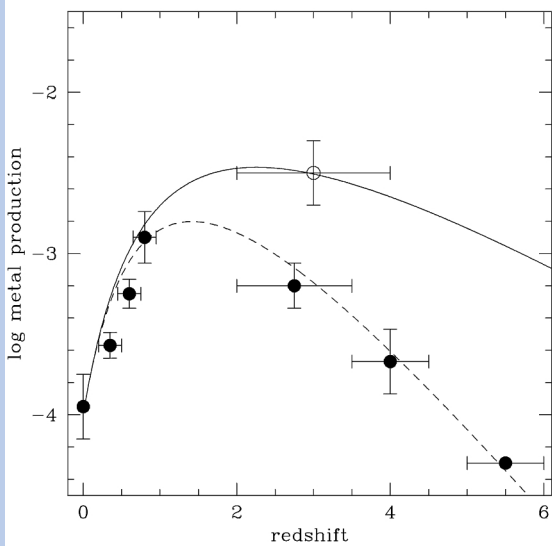


Figure 25. Optical and UV estimates of star formation rate (filled circles) and the SCUBA submillimeter measurement (open circle) as a function of redshift.

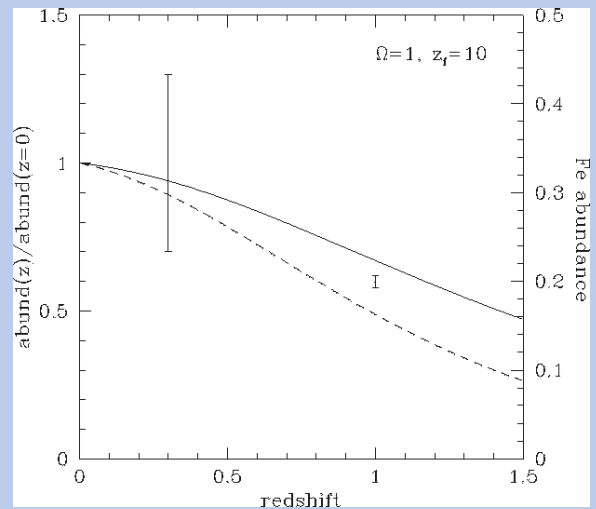


Figure 26. Evolution of ICM metallicity for the two functions shown in Figure 25 that pass through the optical/UV (dashed curve) and submillimeter (solid curve) estimates of star formation rate. The large error bar shows a typical 90% confidence range for an ASCA observation of a cluster at  $z = 0.3$ , the small error bar an estimated 90% confidence range for a 50 ks Constellation-X observation of a cluster at  $z = 1$ .

expected evolution of cluster metal abundance for star formation histories corresponding to functions that pass through the optical and submillimeter high redshift points of Figure 25. The small error bar in Figure 26, representing the Constellation-X measurement of the metallicity of a single cluster at a redshift of 1, shows the expected impact on determining star formation history via observations of the ICM with Constellation-X. We expect to extend such studies substantially further by using Constellation-X to measure abundances for many clusters to redshifts beyond 2.

### 3.2.2 Galaxies and the Intergalactic Medium

#### Detecting the “Missing Baryons” in the Intergalactic Medium

One of the fundamental questions in cosmology is that of the baryon content of the Universe. Recent observations of the Lyman  $\alpha$  forest (i.e., the intergalactic medium at high redshift) show that at  $z \sim 3-4$  most of the baryon content predicted from Big Bang nucleosynthesis calculations is in the IGM. However, at lower redshifts, the baryon content found in stellar systems, neutral hydrogen and X-ray emitting gas in clusters of galaxies (Fukugita, Hogan, and Peebles, 1998) is roughly one order of magnitude less than the predicted value. Given the strong constraints on the baryon content in the Universe from Big Bang nucleosynthetic

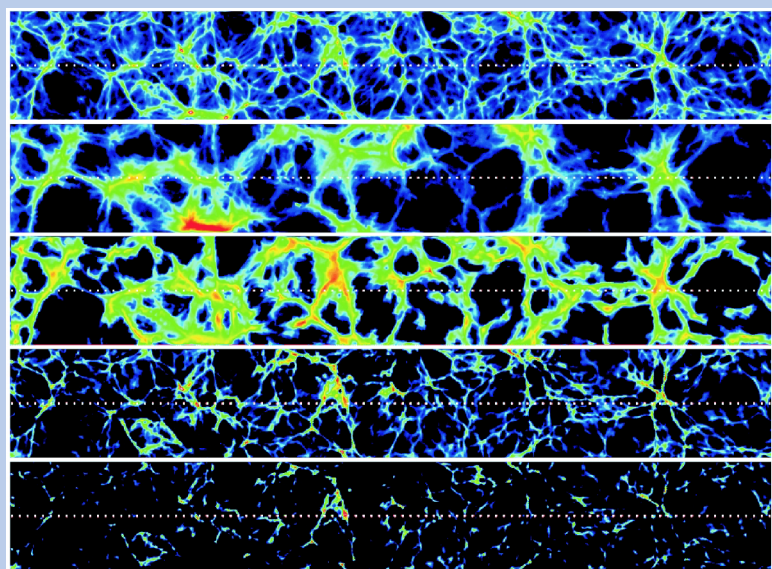


Figure 27. This figure shows a slice of a numerical simulation of IGM at low redshifts along a random line of sight. Rows from top to bottom are as follows: O VII density, O VIII density, metallicity, temperature, and total gas density. From Hellsten, Gnedin, and Miralda-Escude (1998).

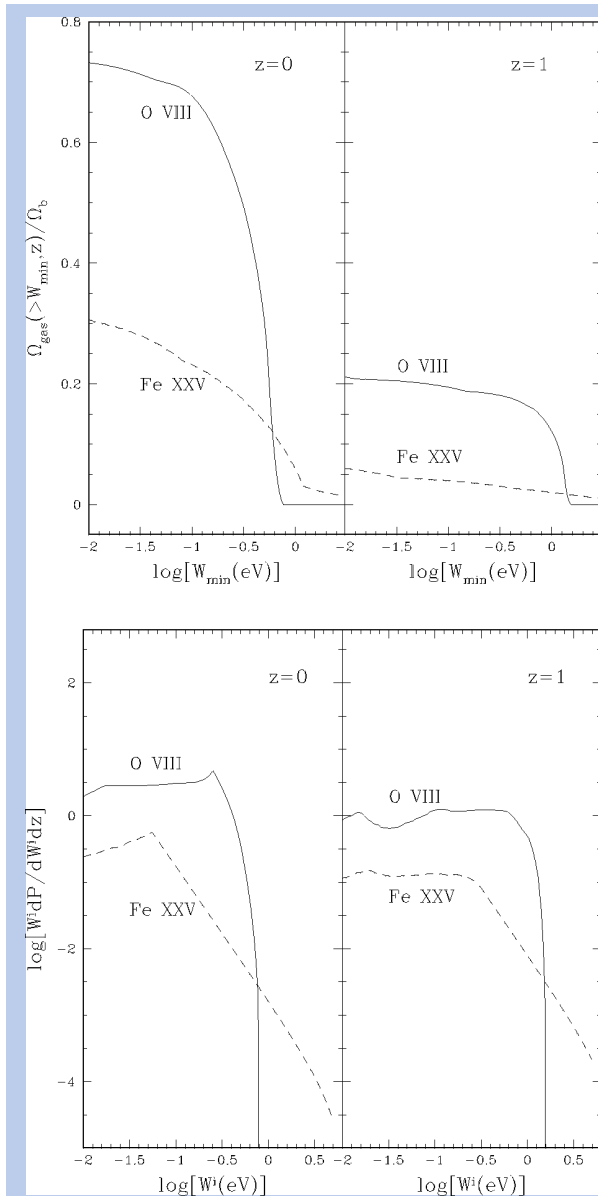


Figure 28. From Perna and Loeb (1998). The top panel shows the fraction of baryons in groups or clusters of galaxies that can be probed by an X-ray telescope with equivalent-width sensitivity  $W_{\min}$  to absorption lines. The solid curve refers to absorption by the strongest resonant transition of O VIII (at  $0.654/(1+z)$  keV, where  $z$  is the absorption redshift), while the dashed curve corresponds to the strongest resonant absorption by Fe XXV (at  $6.7/(1+z)$  keV). The bottom panel shows the probability for observing an absorber equivalent width  $W^i$  per unit redshift per logarithmic equivalent width interval as a function of equivalent width.

considerations and the high  $z$  measurements, it is clear that most of these “local” baryons remain unaccounted for. Where have the baryons gone?

Perhaps most of the “missing baryons” are in a form that has thus far been difficult to detect. This belief is strengthened by detailed numerical large-scale structure simulations (e.g., Cen & Ostriker, 1998) which predict that most of the missing baryons are in the IGM, with temperatures ranging from  $10^5$  K to  $10^7$  K, as influenced by QSO photoionization and shocks from large-scale gravitational infall. The presence of this gas in the IGM can be detected via high resolution spectroscopy revealing absorption lines of the metals against the spectra of background objects such as quasars. Because the gaseous material participates in the Hubble expansion of the Universe, the sites producing the most readily detectable lines will be structures that have collapsed or are collapsing, such as galaxy groups or the outer parts of galaxy clusters. Due to the inferred temperature range of the gas and the background photoionization field, H, He, and other low ionization potential species are very highly ionized and do not produce detectable absorption lines in the optical or ultraviolet regions. However, the IGM gas will be visible in the soft X-ray region through resonance lines of the most common metals, notably OVII and OVIII at 574 eV and 654 eV, respectively.

The maximum signal-to-noise ratio of the predicted absorption signal,  $S/N$ , is limited by photon counting statistics and requires a quasar flux at the line energy  $E$

$$F_E \geq \frac{E \left(\frac{S}{N}\right)^2 \Delta E}{A Q W_{\min}^2 t},$$

where  $\Delta E$  is the width of the spectral resolution bin of the detector,  $A$  is the collecting aperture of the telescope,  $Q$  is the quantum efficiency of the detector, and  $t$  is the integration time of the observation. The future Constellation-X telescope with its planned effective area of  $QA \sim 3,000 \text{ cm}^2$  and resolution of  $\Delta E = 2 \text{ eV}$  at the energy  $E \sim 0.6 \text{ keV}$  could therefore detect an OVIII line with an equivalent width  $W_{\min} = 0.1 \text{ eV}$  at a signal-to-noise ratio  $S/N = 5$  after  $t = 2 \times 10^5$  seconds of integration on a quasar with  $F_E > 8 \times 10^{-12} \text{ erg cm}^{-2} \text{ s}^{-1} \text{ keV}^{-1}$ . Given the number counts of bright quasars and their typical X-ray spectra, there should be several tens of such quasars above the necessary flux threshold across the sky. Figure 28 therefore implies that Constellation-X will be able to probe up to 70% of the hot gas in the outskirts of groups or clusters of galaxies through the OVIII resonant absorption line.

The presence of the warm IGM can also be detected in emission. Figure 29 shows a simulated 200 ks Constellation-X observation of the Galactic foreground plus the intergalactic medium in emission from O VII and O VIII ions. The IGM is modeled by a single thermal component of temperature 0.3 keV and redshift 0.04. The solid line represents the model for the Galactic emission alone (characterized by thermal emission at two temperatures: 0.1 and 0.3 keV). For any random direction, neither the redshift nor emission measure of the IGM is known, but with numerous pointings around the sky, detailed numerical simulations predict that IGM emission should be well-determined.

### Abundances in Galactic Halos

Galaxy halos are an important link between galaxy environments and the IGM. For galaxies with moderate redshift, their outer regions often extend out to 100 kpc and can frequently be seen in absorption against background quasars. Until now, the study of galaxy halos via quasar absorption lines (e.g., Steidel et al., 1994) has been possible primarily for  $z > 0.2$  objects because of the lack of availability of appropriate UV absorption lines (e.g., Mg II, CIV, and Lyman- $\alpha$ ) for lower redshift objects. UV data are also insensitive to a wide range of ions and so the total column densities and abundances derived from UV measurements depend on chosen models for ionization balance. Measurements in the X-ray band are more reliable since they do not depend on ionization state. Examining the ROSAT archival data, there are more than 300 X-ray bright galaxies for which such measurements can be made and about 4,000 quasars available to probe their foreground galactic halos (to a sensitivity threshold of  $\sim 10^{-12}$  ergs  $\text{cm}^{-2} \text{s}^{-1}$  for a background quasar). Constellation-X will determine the total column density (independent of ionization state) for H, He, and O for objects where the total column (HI) is greater than  $10^{20} \text{ cm}^{-2}$ , and will also determine the sum of H and He abundance for galaxies within  $z < 0.3$  to 4% accuracy and oxygen abundances for galaxies with  $z < 0.7$  to 10% accuracy.

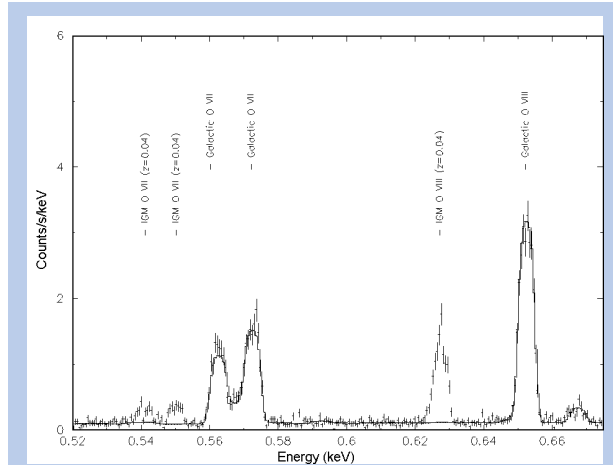
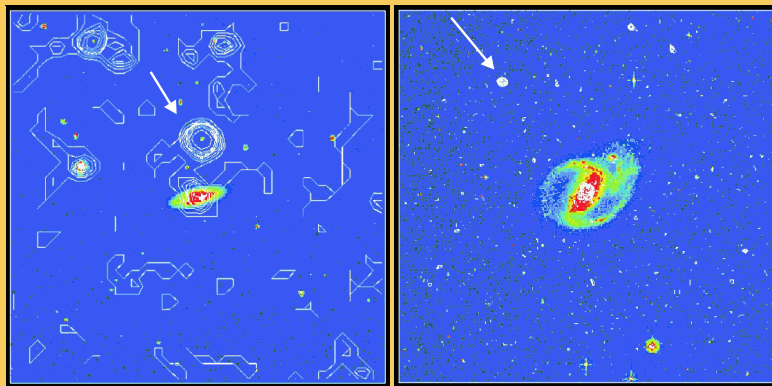


Figure 29. A 200 ks simulated Constellation-X observation of the Galactic foreground plus the IGM in emission from O VII and O VIII. The solid line represents the model for the Galactic emission only.

X-ray contours overlaid on the optical images of two nearby galaxies (NGC 3067 on the left and NGC 1097 on the right) whose halos will be probed by Constellation-X. Arrows point to the location of the background quasars (both of redshift  $\sim 0.5$ ). The sight line to these galaxies have typical HI column densities of few times  $10^{20} \text{ cm}^{-2}$  required for detectability of absorption features. X-ray contours are obtained via ROSAT while the optical images are from the Palomar All Sky Survey.



Constellation-X will also observe thermal emission from starburst-driven winds. By studying the chemical composition of these winds, it will be possible to trace the evolution of the enrichment of the IGM (Figure 18).

### Dark Matter Distribution in Spiral Galaxies

One of the most striking discoveries of astronomy has been that most of the matter in the Universe is non-luminous. While this matter can not be directly “seen,” its presence and distribution can be indirectly inferred via its gravitational potential. The underlying mass distribution of a gravitationally bound system is reflected in its kinematics. Indeed, the

existence of *dark matter halos* in spiral galaxies is proven by the shape of the rotation curves of cold gas and stars, particularly in the outer regions of the disk (e.g., Faber & Gallagher, 1979). Since the stars and gas are heavily confined to the plane of the galaxy, these rotation curves are a sensitive probe of only two dimensions of the distribution of dark matter.

Constellation-X can determine the shape of the mass distribution in all three dimensions through observations of galactic X-ray emitting gas and thereby determine the shape of the dark and luminous matter. Hot gas surrounding spiral galaxies has already been mapped in several edge-on galaxies by Einstein and ROSAT (e.g., Bregman & Houck, 1997). This hot material is supported vertically by thermal pressure and radially through a combination of thermal pressure and centrifugal force. By measuring the temperature and density distribution of the gas as well as its rotational velocity, we can uniquely determine the gravitational potential of the galaxy, which is fundamental to understanding the structure and formation of these systems. Constellation-X will measure not only the temperature and density distribution of the X-ray halos of spiral galaxies but also the rotational velocity of the gas. The expected rotational velocities, based on disk measurements are of order  $\sim 300 \text{ km s}^{-1}$  and so for kinematic studies line centroids must be measured to  $\sim 1 \text{ eV}$ , corresponding to a detector resolution of 5 eV, well within Constellation-X capabilities. By doing so, Constellation-X will be the first observatory to be able to probe the three-dimensional distribution and nature of the dark matter in spiral galaxies.

As a case study, we show a simulated observation of the edge-on spiral galaxy NGC 891. ROSAT and ASCA (Bregman & Houck, 1997) have mapped the hot gas surrounding this galaxy and find that the halo of NGC 891 has a total X-ray flux of  $3 \times 10^{-13} \text{ ergs cm}^{-2} \text{ s}^{-1}$ , a temperature of 0.35 keV, an abundance of 0.5 Solar, and an absorbing hydrogen column density (due to our own Galaxy) of  $10^{21} \text{ cm}^{-2}$ . For this simulation, we assume that Constellation-X will observe 10% of the total flux at each end of the halo (excluding the disk). Figure 30 shows the expected spectrum of the hot halo gas far from the center of NGC 891 in a 50 ks exposure. The solid line shows the model shifted by  $600 \text{ km s}^{-1}$  (assuming a circular velocity of  $300 \text{ km s}^{-1}$ ), demonstrating that the rotational velocity of the halo can be measured. The relative line strengths will be used to determine the temperature and density distribution of the halo gas. Together the velocity and line-strength measurements will define the structure of the mass distribution in spiral galaxies.

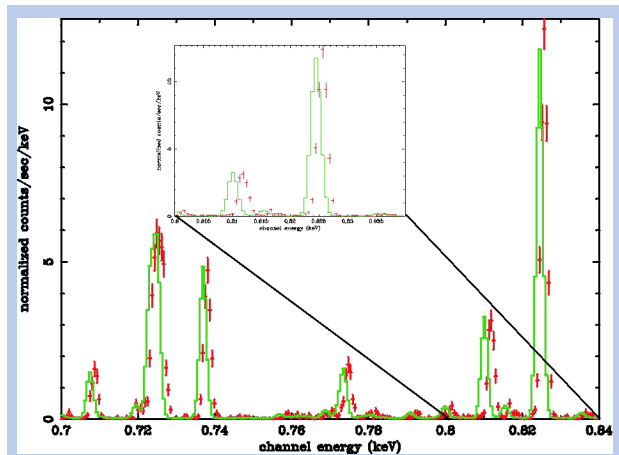


Figure 30. A 50 ks simulated observation of the hot halo gas in the edge-on spiral galaxy NGC 891. The solid line represents the model for the hot gas except that it has been shifted by  $600 \text{ km s}^{-1}$  (i.e., assuming that the halo has a circular velocity of  $300 \text{ km s}^{-1}$ ). The insert shows a zoom-in of the spectrum about 0.8–0.84 keV energy range.

### 3.2.3 Stars, Supernovae, and the Interstellar Medium

#### The Composition of the Interstellar Medium

The composition of the Galactic interstellar medium (ISM) is of fundamental concern since it reflects the star formation history and the creation of the heavy elements in the Milky Way. For these reasons, ISM abundance measurements are one of the central themes of optical and ultraviolet astronomy, with composition being measured by emission lines in HII regions (e.g., Osterbrock, Tran, and Veilleux, 1992) or by absorption lines toward hot stars (Savage and Sembach, 1996). Despite the power of these methods, each is limited by model-dependent assumptions. For H II regions, it is necessary to adopt a model for the ionizing stellar spectrum and a detailed ionization model (e.g., Alexander and Balick, 1997). Also, corrections for absorption (reddening) due to dust are often substantial for most elements. For absorption measurements toward stars, many lines suffer from optical depth effects, an element may be depleted onto grains, and an ionization model is needed in order to convert the column density in an ionization state to the column for the element as a whole.

High resolution X-ray spectroscopy promises an enormous advance for ISM abundance determinations. The technique is fundamentally different from optical-ultraviolet methods because it uses the photoelectric L or K shell absorption of X-rays toward background sources. Throughout the soft X-ray band, a series of absorption edges occurs for the elements C (0.28 keV), N (0.40 keV), O (0.532 keV), Fe (0.71 keV), Ne (0.867 keV), Mg (1.30 keV), and Si (1.84 keV). For typical values of the Galactic column density,  $1 \times 10^{20}$ – $3 \times 10^{21}$   $\text{cm}^{-2}$ , the opacity of these features make them clearly detectable (Morrison and McCammon, 1983). The opacity increase across the L or K shell edge yields a direct measurement of the column density of a given element. The following are two important advantages to this method that lead to high accuracy abundance measurements:

- ▶ The abundances are independent of depletion onto grains because metals in the dust phase absorb very nearly as though they were in the gas phase.
- ▶ The abundances are effectively independent of the ionization state distribution for an element, thus avoiding photoionization model corrections (e.g., Fe I, Fe II, and Fe III have nearly the same inner shell photoionization cross section).

Because this method is independent of dust effects and photoionization models, it will be possible for the first time to obtain abundances with an uncertainty of order 10% for seven of the most common elements along hundreds of sightlines. Chandra, Astro-E, and XMM will use this method to measure oxygen columns along a handful of sightlines. However, studies of the other six elements, and for oxygen along many sight lines is only possible with the increased sensitivity provided by Constellation-X.

X-ray absorption studies will reveal the relative ionization states of the gas along the line of sight to a background quasar. This is essential for understanding the structure and properties of the ISM. The actual ionization state of an element leads to a small shift in the energy of the absorption edge, so for each element, a series of edges will be observed whose relative strengths yield the distribution of the ionization state of the elements along the line of sight. This high-precision measurement requires excellent spectral resolution coupled with high signal-to-noise, which will be possible only with Constellation-X.

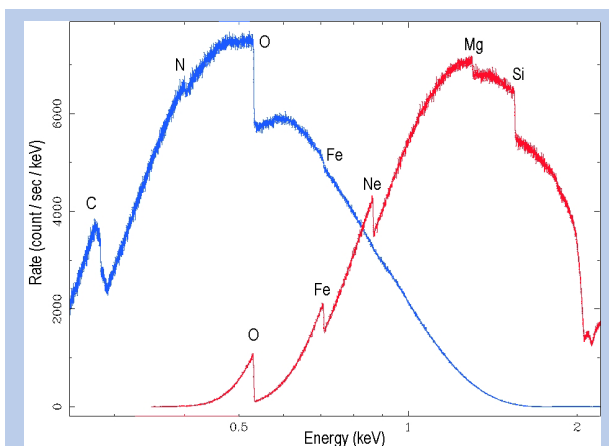


Figure 31. Spectra of two typical quasars, one observed with the transmission grating (left) and the other with the quantum calorimeter (right) onboard Constellation-X. For the grating, the absorption column is  $5 \times 10^{20}$   $\text{cm}^{-2}$ ; for the calorimeter, the absorption column is  $5 \times 10^{21}$   $\text{cm}^{-2}$ . Abundances can be measured accurately from the absorption edges.

Figure 31 illustrates these points by showing simulations of spectra from two moderately bright quasars, which are seen through two different hydrogen column densities in the ISM. Abundance determinations of the ISM via this technique is similar to abundance determination of Galactic halos in external galaxies via quasar absorption lines as discussed in a previous section.

### Supernova Nucleosynthesis: Beyond the Alpha Elements

Nearly all elements heavier than helium are created in the interiors of stars via nucleosynthesis. They are dispersed into interstellar space via stellar winds and supernova explosions (see also Figure 18). Much of this material ultimately coalesces into subsequent generations of stars, possibly with planetary systems. The relative abundances of the elements created and dispersed in this way depend on the mass of the given star and the mechanism by which it explodes. A supernova explosion produces a remnant in which the dispersed material is heated to tens of millions of degrees, and at these temperatures, the highly ionized nucleosynthesis products emit radiation primarily in the form of X-ray lines. Because each element produces a unique set of lines, X-ray spectroscopy will identify the nucleosynthesis products and determine the amount of each generated by a particular supernova.

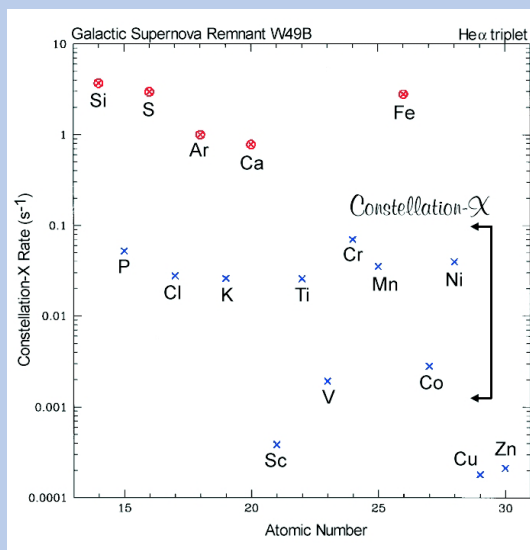


Figure 32. The Constellation-X count rates for the sum of the He-like triplet lines as a function of atomic number for all elements from Si to Zn in W49B. The five circled points near the top of the plot correspond to the astrophysically abundant elements Si, S, Ar, Ca, and Fe. The next lower set of points are for the elements P, Cl, K, Ti, Cr, Mn, and Ni.

Measurements from existing X-ray observatories have verified the general theoretical scheme of how stars sufficiently massive to explode synthesize the most abundant elements. With Chandra, XMM, and Astro-E, it will be possible to measure these abundances more accurately; however, the spectral capabilities of these missions for supernova remnants will be limited by the fact that these objects are extended and thus unsuitable for high spectral resolution observations using gratings. The 2 eV resolution and throughput of the Constellation-X calorimeter will revolutionize this research area. It will allow detections of X-ray lines one hundred times weaker than those detectable by Chandra or XMM, and therefore will allow abundance determinations of many more elements.

We consider the Galactic SNR W49B as an example. The ASCA CCD spectrum of this remnant (with a 2–10 keV flux of  $\sim 7 \times 10^{-11}$  ergs  $\text{cm}^{-2}$   $\text{s}^{-1}$ ) shows bright line complexes from K-shell transitions of He-like and H-like ions of Si, S, Ar, Ca, and Fe. In an observation of merely 1500 s, Constellation-X will be able to detect (at the  $10\sigma$  level) and resolve the weakest of the He-like lines for these elemental species. Figure 32 illustrates the Constellation-X count rates for the He-like complex as a function of atomic number for all elements from Si to Zn. Highly significant detections of the odd-Z elements in the group from P to Ni shown in the figure will be obtained by Constellation-X in less than 20,000 s, while the weakest lines from the least abundant species (Sc, V, Co, Cu, and Zn) may be detected in observations of  $10^5$  s.

As another example, Figure 33 shows portions of spectra from simulated 100 ks Chandra ACIS and Constellation-X observations of the young supernova remnant N103B in the Large Magellanic Cloud. The Chandra simulation does not include the high energy transmission grating since the source is extended. The simulations include the full complement of nucleosynthesis products that are expected to be produced in a type Ia supernova explosion (i.e., the result of runaway thermonuclear burning in a white dwarf that has exceeded the Chandrasekhar mass limit). The ACIS CCD will resolve only the strong line blends of Ca, Ar, and Fe. The Constellation-X calorimeters will resolve the details of

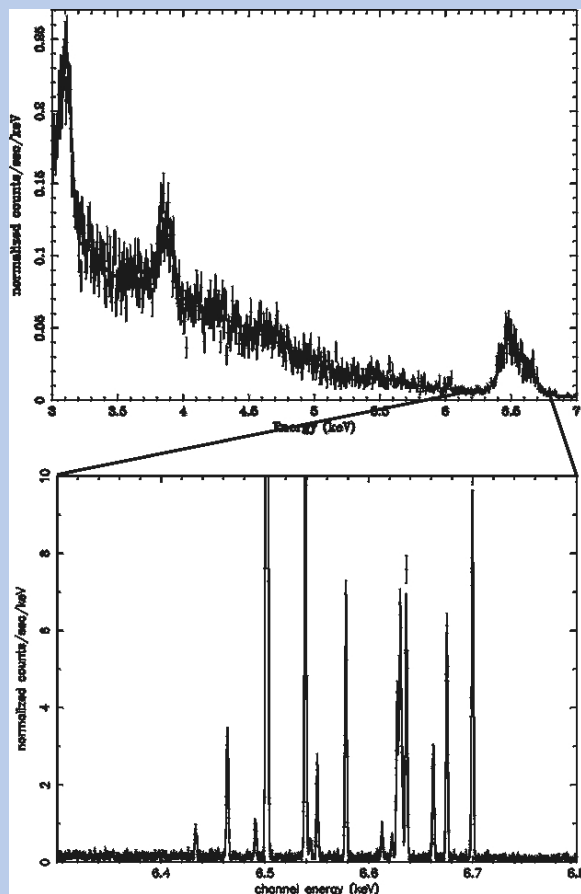


Figure 33. Simulated 100 ks Chandra ACIS (top panel) and Constellation-X (limited to the narrow 6.3–6.8 keV range, bottom panel) observation of the young supernova remnant N103B. With Constellation-X, the iron K complex can be resolved.

the iron K complex and the weak lines corresponding to elements such as Cl, K, Ti, Cr, and Mn will be detectable for the first time. This will allow more complete tests of the theoretical models that seek to explain nucleosynthesis during stellar evolution and supernova explosions.

## Doppler Imaging of Active Binary Star Systems

Stellar coronae often exhibit line-rich X-ray spectra. X-ray spectroscopy with Constellation-X will allow us to derive very sensitive constraints on physical conditions in the coronal plasmas. The spectrometers on Chandra, XMM, and Astro-E will require long exposures to accumulate high-quality spectra of even the brightest stars. The much higher throughput of Constellation-X is required to reach the fainter (more distant and/or less luminous) systems and to obtain high quality time-resolved spectra.

As a specific example, we focus on eclipsing stellar binary systems, for which we can use the morphology of the X-ray light-curve to infer the spatial structure of the coronal plasma on either or both of the component stars. While the duration of an eclipse yields information on the extent of the emission associated with the eclipsed star, there are too few constraints from the lightcurve alone to give a unique solution. With the spectral resolution and large collecting area available with Constellation-X, we will for the first time be able to break this degeneracy by using velocity information to map the coronal structures on the underlying stars. This technique, called Doppler imaging, has been utilized in the optical and UV bands to map the location of photospheric features, but only by combining these data with X-ray observations can we determine the full three-dimensional structure of the stellar atmosphere. For the Fe XXV resonance line at 6.7 keV, a resolution of 2 eV gives a velocity resolution of  $90 \text{ km s}^{-1}$ , which will enable us to study close binary systems like AR Lac. This system contains a G2IV star and a K0IV star that are rotationally phase-locked to the two-day orbital period. During a long EXOSAT exposure in 1984 (Figure 34), a large fraction of the total X-ray emission came from spatially compact regions, probably associated with bright chromospheric plages, on each star. The strong Fe XXV resonance line is clearly split into two components due to the differential Doppler shifts of the two stars.

The large effective area of Constellation-X will enable the first high quality spectra of the Fe K line from this system in an exposure short compared to the orbital period. For a single orbital period, dozens of time-resolved spectra can be obtained. These will enable a study of coronal structures with spatial dimensions much smaller than the stellar radii. Constellation-X can isolate the Fe XXV resonance line (and other strong resonance lines such as Ca XIX at 3.90 keV) of each star, and determine the coronal abundances. Also through the use of plasma diagnostic line combinations, the densities of the individual active regions can be directly determined and compared with the densities inferred from Doppler imaging and eclipse mapping.

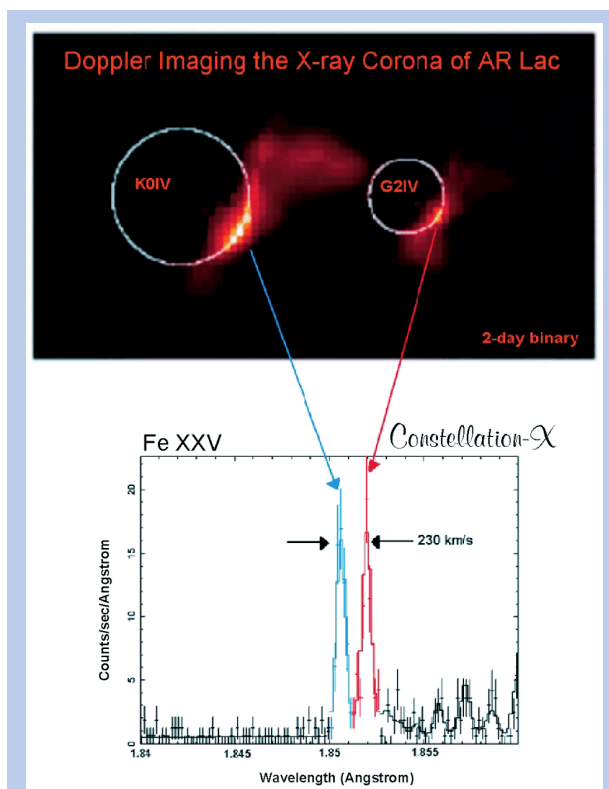


Figure 34. The top panel shows an eclipse-mapping spatial deconvolution of the coronae of the RS CVn binary AR Lac as derived from a long EXOSAT exposure. The lower panel shows a simulated 20 ks Constellation-X observation of AR Lac, assuming that the exposure was centered on orbital quadrature when the velocity separation of the two stars in this binary system is at its maximum value of  $230 \text{ km s}^{-1}$ . For simplicity, it is assumed that each star contributes equally to the total X-ray emission. The strong Fe XXV resonance line is clearly split into two components due to the differential Doppler shifts of the two stars. Figure courtesy of Steve Drake.

### 3.2.4 Solar System X-rays

Besides the Sun (and objects such as the Moon that shine by fluoresced sunlight), the known X-ray sources in our solar system are the Earth, Jupiter, and, as recently discovered, comets. Compared with the cosmic sources discussed so far, these planetary and cometary sources are extremely weak. Nonetheless, the X-rays that emanate from them are an intriguing manifestation of the interaction of these bodies with the magnetized plasma medium in which they are embedded and offer important clues as to the nature of this interaction. Analyses of these emissions can help advance our understanding of certain basic plasma and plasma-neutral processes that are important within our solar system and, by implication, in extra-solar planetary systems as well. This is particularly so when the analysis is correlated with in-situ fields and particles data and with remote-sensing observations at other wavelengths.

Terrestrial X-rays were discovered in the 1950s. X-rays from Jupiter were first detected in 1979 with the Einstein observatory (Metzger et al., 1983) and have been regularly observed with ROSAT since 1992 (e.g., Gladstone et al., 1998). In the case of both the Earth and Jupiter, X-ray emissions are generated by the precipitation of energetic magnetospheric particles into the dense neutral gas of the planetary atmosphere. Terrestrial X-rays are known to be bremsstrahlung emissions produced by energetic auroral electrons. The excitation process responsible for Jupiter's X-ray emissions, on the other hand, has not yet been conclusively identified. The emissions could, as at Earth, be bremsstrahlung produced by energetic electron precipitation. However, this is considered unlikely to be the dominant mechanism because it would require a power input into the atmosphere 2–3 orders of magnitude greater than that estimated from the intensity of the UV auroral emissions observed for Jupiter by Voyager (Metzger et al., 1983). A more plausible explanation, one supported by theoretical and modeling studies using limited ROSAT PSPC data, is that the Jovian X-rays are line emissions from precipitating energetic (keV per nucleon) sulfur and oxygen ions that become highly ionized and excited through their interaction (electron stripping, charge transfer, direct excitation) with Jupiter's neutral upper atmosphere (Waite et al., 1994; Cravens et al., 1995). Because of the limited spectral resolution and sensitivity of the Einstein and ROSAT instruments, it has not been possible to establish whether the Jovian X-rays are bremsstrahlung or line emissions.

While Chandra observations of Jupiter may reveal whether energetic electron or heavy ion precipitation is responsible for exciting the emissions, full understanding of the magnetospheric processes involved in the acceleration, transport, and loss of auroral particles will require spectra with a much higher signal-to-noise ratio. If, as is expected, energetic heavy ion precipitation is found to be the process by which the Jovian X-rays are excited, then the emissions can yield

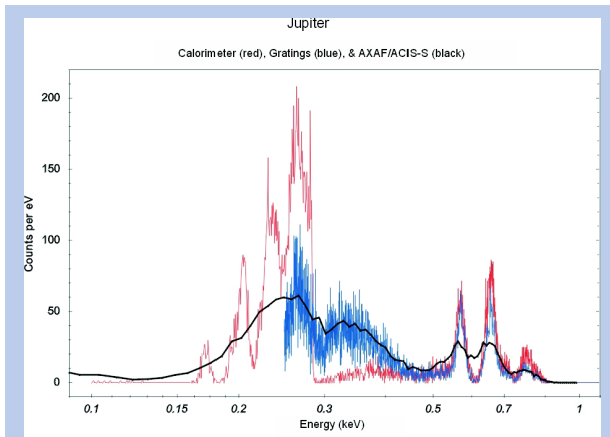


Figure 35. Simulated calorimeter (red) and grating (blue) spectra vs. energy for a 50 ks Constellation-X observation of Jupiter. The ion-precipitation model with flux at Earth of  $1.4 \times 10^{-13}$  ergs  $\text{cm}^{-2} \text{s}^{-1}$  (as typically measured by ROSAT) is assumed. Each peak is a blend of lines from various charge species of oxygen and sulfur. The black curve shows a simulated 50 ks observation of Jupiter with Chandra/ACIS-S (multiplied by a factor of 10).

information about the relative contributions of the sulfur and oxygen ions to the X-ray excitation and the charge state distribution for each species. In addition, deceleration and thermalization of the precipitating ions is expected to lead to appreciable emission line broadening, from which the energy spectra of the incident particles may be deduced. Knowledge of the ion composition, charge state distributions, and energies particularly when correlated with in situ field and particle data and radio measurements of synchrotron emission from Jupiter's radiation belt, etc., can in turn be used to identify magnetospheric source regions and to elucidate the microphysics of ion acceleration, transport, and loss in Jupiter's massive, co-rotation-driven magnetosphere. As illustrated by the simulated spectra in Figure 35, Constellation-X will have the superior sensitivity and spectral resolution necessary to provide the high signal-to-noise ratio spectra that will allow planetary scientists to fully exploit the information contained in Jupiter's X-ray emissions.

Cometary X-rays were discovered only recently, with the 1996 ROSAT detection of X-ray emissions from comet C/Hyakutake (Lisse et al., 1996). Several excitation

processes have been proposed to explain these unexpected emissions (Krasnopolsky, 1998). Of the suggested mechanisms, the most likely is one proposed by Cravens (1997) on the basis of his theoretical work on Jovian X-ray production: charge transfer between high-charge-state heavy ions in the solar wind and the neutral coma, which produces highly excited ions that then emit X-ray and EUV photons when they de-excite. Given the apparent importance of charge transfer in the generation of X-ray emissions at Jupiter and comets, it is not unreasonable to speculate that this process occurs elsewhere in the solar system as well (e.g., Venus, the Galilean satellites), resulting in the (possibly detectable) production of soft X-rays. Analyses of high signal-to-noise ratio spectra obtained by Constellation-X together with comparative studies of X-ray generation at Jupiter can help elucidate the mechanisms of X-ray production at comets and other possible solar system X-ray sources.

# 4 The Technology

*Substantial but affordable advances in technology . . .*

## 4.1 Introduction

The fundamental science questions to be addressed by Constellation-X require a substantial increase in effective area, energy resolution, and energy bandpass. To accomplish these ambitious increases at an affordable mission cost, we must introduce new approaches for the development and operation of the mission and exploit technical advances from other programs as well. An essential feature of this concept involves minimizing cost and risk by building identical, modest satellites to achieve a large area.

Baseline Mission Characteristics	
Minimum effective area:	15,000 cm <sup>2</sup> at 1 keV 6,000 cm <sup>2</sup> at 6.4 keV 1,500 cm <sup>2</sup> at 40 keV
Minimum telescope angular resolution:	15" HPD from 0.25 to 10 keV 1' HPD at about 10 keV
Minimum spectral resolving power: (E/ $\Delta$ E)	300 from 0.25 to 6.0 keV 3000 at 6 keV 10 at 40 keV
Maximum Source Count Rate	$\sim 10^4$ counts/sec
Band Pass:	0.25 to 40 keV
Diameter Field of View:	2.5' < 10 keV 8' < 25 keV
Mission Life:	3 years minimum 5 years goal

Key technologies relating directly to the Constellation-X science instruments and spacecraft include state-of-the-art X-ray mirrors, multilayer coatings, spectrometers, low-energy and high-energy X-ray detectors, cryogenic systems, extendible optical benches, lightweight satellite buses, and advanced communications systems. Development efforts in each area will benefit a variety of NASA programs including Constellation-X.

The specific Constellation-X mission requirements (see above) that drive the Technology Roadmap are its large effective area (15,000 cm<sup>2</sup> at 1 keV), high spectral resolution ( $R \sim 300-3000$ ), and broad energy bandpass (0.25–40 keV). These requirements can be met by using replicated optics with reflection gratings, charge-coupled device detectors (CCDs), quantum microcalorimeters, and cadmium zinc telluride (CZT) or silicon hard X-ray detectors.

## 4.2 Spectroscopy X-ray Telescopes

Constellation-X uses a Wolter Type I design of nested, grazing-incidence X-ray mirrors to focus X-rays. Although the design uses many more mirror shells than Chandra, the optical figure requirement is much lower. Replication techniques will be used in which the shell, or segments of a shell, are duplicated from a precisely shaped mandrel. This

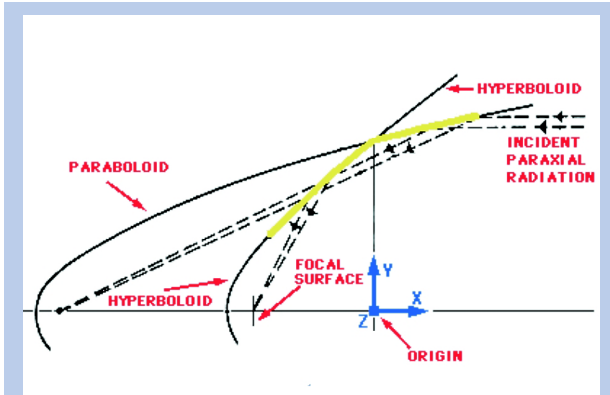


Figure 36. Illustration of parabolic-hyperbolic focusing of incident X-rays using grazing incidence mirrors. The colored segments of the curves represent the physical surfaces of the optics. The angles have been greatly exaggerated to fit the schematic to the page.

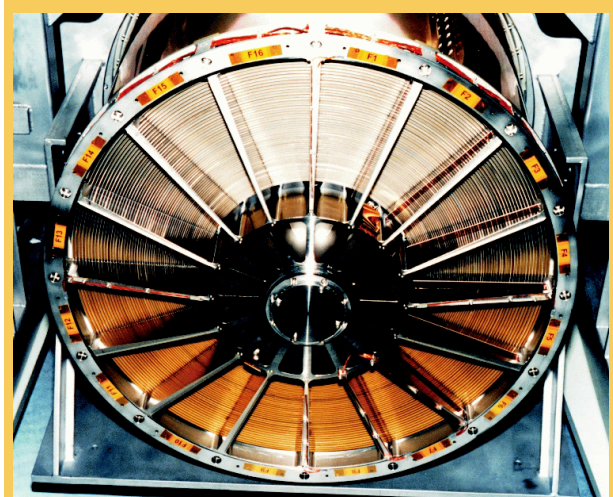
has the advantage that many mirror elements can be made from the same mandrel thus reducing costs. The Constellation-X mirror program is pursuing both a closed shell and a segmented shell approach to produce lightweight, high throughput X-ray optics. The mission objectives can be met with four mirror assemblies, each having a diameter of 1.6 m, similar to that of Chandra but with a much greater overall area.

Two approaches are currently being considered for the X-ray mirrors for the Spectroscopy X-ray Telescope (SXT). One approach uses replicated shells, in a manner similar to XMM, Jet-X, and SAX, while the alternative approach uses replicated segments similar to Astro-E (with heritage from ASCA and BBXRT). Both techniques promise to satisfy the Constellation-X scientific requirements. However, neither currently meets all of the Constellation-X requirements (low weight combined with 15" HPD). A substantial technological investment is required either to improve the angular resolution of the

replicated foil segments or to reduce the weight of the replicated shells.

#### 4.2.1 Replicated Shells

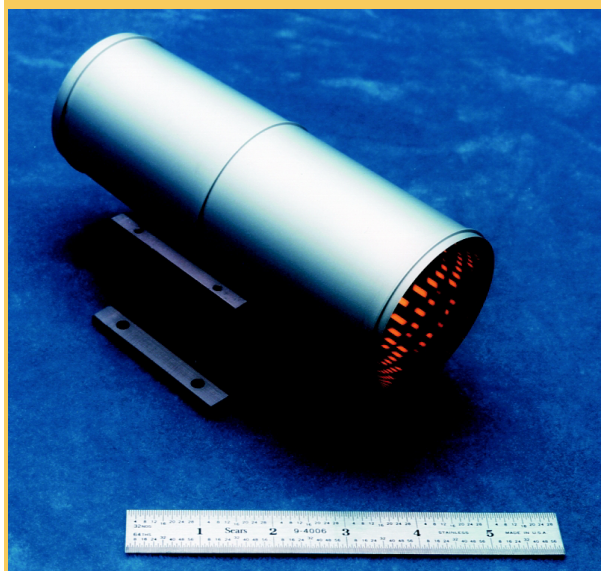
The state of the art in replicated shell mirrors is defined by the optics developed by ESA for XMM which have a HPD of 12", slightly better than the Constellation-X target of 15". Each (of three) XMM mirror assembly uses 58 nickel shells electroformed from metal mandrels. The basic approach builds on technology developed for the SAX and JET-X missions by the Osservatorio Astronomico di Brera in Milan, Italy. The weight budget for each set of baseline Constellation-X mirrors is 250 kg, a factor of about 6 less than XMM optics would weigh. The Constellation-X technology development program is directed towards reducing mass to the required value without an unacceptable sacrifice of performance. Various approaches include "integral" and "non-integral" carriers. The "integral" approach is similar to that used by XMM, though using lightweight nickel alloys or thinner nickel shells with stiffening rings. The non-integral approach uses carbon fiber (or silicon carbide or alumina) shells that are fabricated and then, using epoxy, are attached to gold which has been deposited onto the mandrel. The whole assembly is then separated and the shells are imparted with the mandrel finish and optical figure.



View of the back of an XMM mirror module. This is the side from which the photons continue to the detectors in the foci of the mirror shells (or onto the Reflection Grating Arrays).

#### 4.2.2 Replicated Foil Segments

Another method of replicating X-ray optics is the "foil mirrors" technique. The mirror is fabricated in segments of aluminum foil. Gold is deposited onto a glass mandrel and a thin layer of epoxy is used to attach the aluminum foil and lift off the gold. A typical mirror is populated by 100 or more foil reflector pairs. A foil mirror of the size needed for Constellation-X would be within the 250 kg mass budget, but the required spatial resolution has not yet been attained. The best HPD for a completed foil mirror assembly is about 1.5', based on the Astro-E foils. The limiting factor is the



Example of an integral nickel shell with stiffening rings.

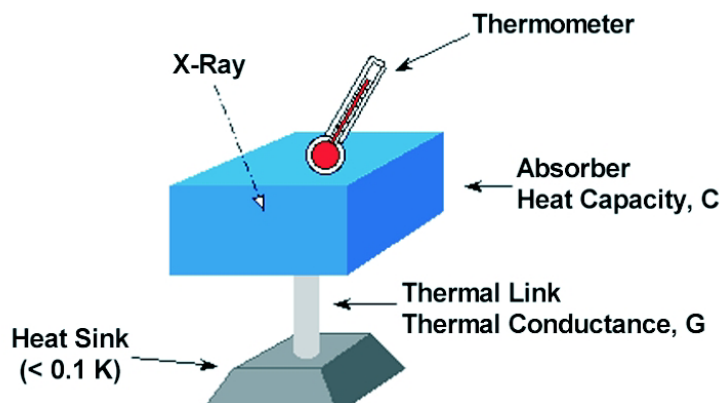
accuracy of mounting the foils, the relatively poor surface quality of the mandrels, and lack of stiffness in the aluminum used as a substrate. To meet the science goals of the Constellation-X mission, the HPD must be improved by a factor of six. The program is pursuing stiffer substrate material, better mounting designs, and higher quality mandrels.

The conical approximation approach replaces Wolter I parabolas and hyperbolas with simple cones. This reduces weight and increases aperture utilization since the thick-walled substrates are replaced by thin foils. The image quality depends on the projected width of the foil reflectors on the focal plane, which in turn is a function of the length of the reflectors and the average grazing angle. If the reflector length and mirror diameter are held constant, then the intrinsic image size improves as the focal length is increased. For an 8 m focal length with a 1 m diameter and 10 cm reflectors, the intrinsic image HPD is 13"; thus in order to meet the spatial resolution requirement for Constellation-X using a conical mirror,

an image quality approaching the theoretical limit must be attained, or the simple conical geometry must be replaced by true parabolas and hyperbolas.

## 4.2 Calorimeters

The low fluxes from celestial X-ray sources require a detector system that has the highest possible detection efficiency. The highest spectral resolution available to date has been provided by dispersive techniques employing gratings or crystal spectrometers. These offer extremely high energy resolution, particularly at low energies, but can have low quantum efficiency or limited energy coverage (for crystals) and may not be suitable for the study of extended sources (for gratings). Non-dispersive spectrometers based on ionization in silicon, such as diodes and charge-coupled devices, have higher quantum efficiency but lower energy resolution due to the statistics of charge production and collection in silicon. In 1982, a new approach to non-dispersive X-ray spectroscopy, based on the measurement of heat rather than charge, was proposed by Moseley et al. (1984). The detector, an X-ray microcalorimeter, works by sensing the heat pulses generated by X-ray photons when they are absorbed and thermalized. The temperature increase indicates the photon energy. This invention combines high detector efficiency with high energy resolution.



Any microcalorimeter must have a low-heat-capacity mass to absorb incident X-ray photons, a weak link to a low-temperature heat sink which provides the thermal isolation needed for a temperature rise to occur, and a

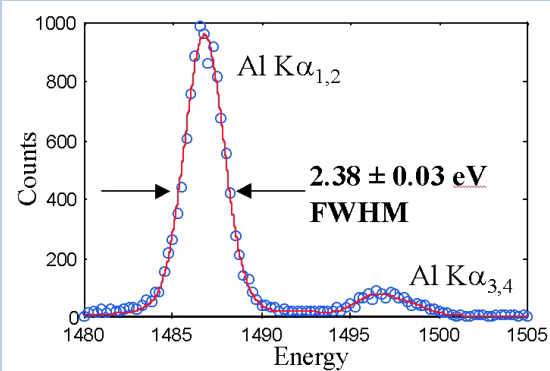


Figure 37. X-ray spectrum measured with TES microcalorimeter, which consists of an Al/Ag superconducting thermometer and a bismuth absorber suspended on a Si<sub>3</sub>N<sub>4</sub> membrane.

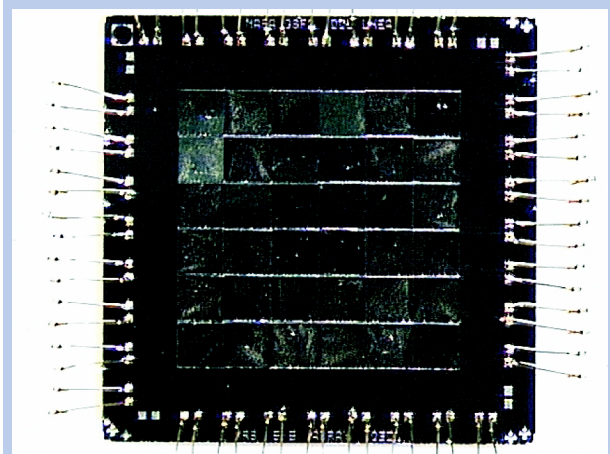


Figure 38. XRS-style 6×6 microcalorimeter array. The HgTe absorbers tile the plane with 93% coverage, obscuring from view the monolithic array of micromachined suspended Si thermistors.

thermometer to measure change in temperature. Specific implementations of the basic calorimeter concept have used a variety of absorbers, suspension schemes, and thermometers. To date, the best performance has been achieved using thermistors, for which a change in resistance accompanies a change in temperature. Resistive thermometers can be characterized by their sensitivity,  $\alpha = d(\log R)/d(\log T)$ , where R is the resistance and T is the temperature. In an ideal thermistor-based calorimeter, for which the dominant noise sources are Johnson noise and thermal fluctuations across the weak link, the energy resolution,  $\Delta E$ , scales as  $T\sqrt{C/|\alpha|}$ , where C is the total heat capacity. This resolution is independent of energy to the extent that the temperature excursion is small compared with the operating temperature. Presently there are two types of resistive thermometers used in microcalorimeters: doped semiconductor thermistors and superconducting thermometers designed to be operated within the temperature range of the superconducting transition.

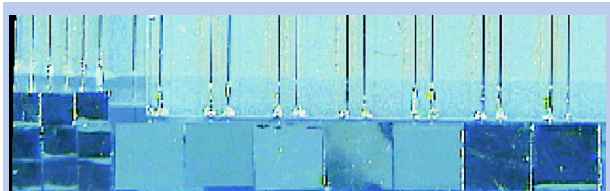


Figure 39. Array of microcalorimeters formed by suspending NTD Ge thermistors with Sn absorbers from sapphire substrates using bond wires.

The X-Ray Spectrometer instrument (XRS) on Astro-E will be the first X-ray microcalorimeter spectrometer in orbit when it is launched early in the year 2000. Its 32-element array of  $\sim 0.4 \text{ mm}^2$  pixels uses HgTe absorbers, micro-machined silicon suspensions, and ion-implanted silicon thermistors. The detector is efficient from 0.3–12 keV and provides  $\sim 12 \text{ eV}$  resolution at 6 keV (and somewhat better at lower energies). Similar devices optimized for use below 1 keV (thinner absorbers) have demonstrated  $\sim 6 \text{ eV}$  resolution. Microcalorimeters of neutron-transmutation-doped (NTD) germanium thermistors paired with tin absorbers have provided 7 eV resolution at 6 keV and 5 eV resolution at 1.5 keV. Arrays of NTD-based calorimeters are now being made. Low-noise read-out of high-resistance semiconductor thermistors is achieved through quiet Junction Field Effect Transistors (JFETs).

Superconducting transition-edge sensors (TES) can achieve values of  $\alpha$  more than an order of magnitude higher than semiconductor thermistors. Because they are only sensitive in the limited temperature range of the superconducting transition, however, the heat capacity must be large enough to keep the temperature within the transition upon the absorption of the highest energy X-ray of interest in a particular experiment. Thus, for the astronomical X-ray band, the theoretical resolution for TES-based and semiconductor-based microcalorimeters is about the same. The advantage of TES-based devices is that the larger heat capacity budget permits a wider choice of absorber materials. Normal metals, off-limits to semiconductor-based calorimeters, can be used with TES-based calorimeters, exploiting the rapid and efficient thermalization that occurs in metals. This permits the design of a fast device. Electrothermal feedback,



**Turbo-Brayton Cooler**

present in any resistive calorimeter because the bias power into the device changes as its resistance changes, can be particularly dramatic in a high- $\alpha$  device. Voltage-biasing of a TES produces extreme negative feedback, permitting stable biasing within the narrow superconducting transition and actually making the recovery time of the thermal pulses faster than the intrinsic thermal time constant. Energy resolution of 4.7 eV at 6 keV has already been demonstrated with a single pixel TES device and 2.38 eV at 1.5 keV with count rates in excess of 400 counts  $s^{-1}$  (Figure 37) on another device. Low-noise read-out of low-resistance transition-edge thermometers is achieved through series arrays of superconducting quantum interference devices (SQUIDs).

Microcalorimeter development for a  $30 \times 30$  element array for Constellation-X is proceeding with the primary emphasis on TES-based devices arrayed on micro-machined silicon support structures. Secondary emphasis is being placed on optimizing and arraying NTD-Ge-based devices. Back-up technologies using epitaxial doped Si and Ge thermometers will also be pursued as a way of combining the reliability of bulk-doping (e.g., NTD Ge) with the ease of making monolithic arrays by micro-machining silicon.

Microcalorimeters require cooling to  $\sim 50$  mK in order to minimize the magnitude of thermal fluctuation noise. Constellation-X must provide the cooling required by the calorimeters within a fairly severe envelope of weight, power, size, and cost constraints. The XRS system on Astro-E consists of solid neon surrounding liquid helium that provides a heat sink for an adiabatic demagnetization refrigerator (ADR). This is the state of the art for such a cooling system. It could be further developed to meet the Constellation-X requirements but would be heavy and have a limited lifetime. A mechanical cooler could be smaller and lighter and operate indefinitely. A design that uses a turbo-Brayton cooler to feed an ADR is a better candidate for Constellation-X.

### 4.3 Gratings/CCD Arrays

At energies above 1 keV, microcalorimeters offer the best promise to achieve adequate spectral resolution ( $E/\Delta E > 500$ ) with high quantum efficiency. However, at lower energies they are inadequate for the mission spectral resolution requirement (see Figure 4). One reason for the degradation in performance of the calorimeters at lower energies is the use of blocking filters to suppress visible and infrared light to reach the detectors. This causes the net quantum efficiency of the microcalorimeters to fall steeply below 1 keV. Furthermore, because the energy resolution of the microcalorimeters ( $\Delta E \sim 2$  eV) is independent of energy, the spectral resolving power,  $E/\Delta E$ , falls linearly below 1 keV. In fact,  $\Delta E \sim 2$  eV is insufficient to resolve key spectral features at energies below 0.5 keV. The soft X-ray spectral range is very line-rich for nearby sources, and becomes increasingly important for more distant sources as bright X-ray K-shell lines get redshifted down in energy.

Unlike the calorimeters, the resolving power of the reflection gratings improves at lower energies. The spectral resolution of the grating is generally limited by the angular resolution of the telescope, which means that it is the wavelength resolution,  $\Delta\lambda$ , that is independent of energy (unlike  $\Delta E$  in the case of microcalorimeters). As a result, the resolving power,  $E/\Delta E = \lambda/\Delta\lambda$ , increases linearly as the energy decreases. Furthermore, both the diffraction efficiency of reflection gratings and the achievable spectral resolution are higher at lower



A sample reflection grating produced via anisotropic etching of a silicon wafer.

energies because of the higher allowable graze angles. Thus, reflection grating spectrometers and microcalorimeters are complementary. The inclusion of both types of instruments on Constellation-X offers an extremely powerful payload for astrophysical spectroscopy across the entire X-ray band from 0.25 to 10 keV.

The baseline reflection grating spectrometer design involves an array of thin reflection gratings mounted at grazing incidence to the beam immediately behind the Spectroscopy X-ray Telescope optics. The grating array covers only half of the telescope shells and is spaced so as to pick off only  $\sim 50\%$  of the light passing through. The remaining 50% of the light from the outer shells, and all of the light from the inner shells, passes undeflected through the grating array to the microcalorimeter at the telescope focus. The light picked off by the grating is dispersed to a strip of CCD detectors offset in the dispersion direction. The gratings are all mounted at the same incident graze angle with respect to the ray passing through grating center, and they are positioned on a Rowland torus which also contains the telescope focus and the CCD detectors. This configuration eliminates the comatic aberrations due to the convergence of the beam intercepted by each individual grating, slightly varying the groove spacing over the length of the grating.

To improve on the XMM heritage, we are investigating the fabrication of reflection gratings via interference lithography on graze-cut (100) silicon wafers. This concept exploits the highly anisotropic etching property of special silicon etches, which stop on the (111) lattice planes, effectively producing grating grooves with atomic smoothness and a high degree of geometry control. Thick silicon substrates will be thinned using chemical etching of buried-oxide parting layers. The resulting thin grating “films” will then be bonded to stiff carrier frames under tension and positioned using precision four-point mounts within an assembly structure. The integrating structure which supports the array will be integrally coupled to a deep, stiff telescope structure that also supports the mirror shells.

For the CCD detectors, we are investigating a resistive-gate design in which a single polysilicon layer is heavily doped in selected regions to produce narrow gates. This design offers a number of advantages over conventional X-ray CCD architectures, including: reduced electrode capacitance leading to lower drive power for the electronics, less susceptibility to radiation damage from protons, and enhanced low energy efficiency in a front-illuminated device.

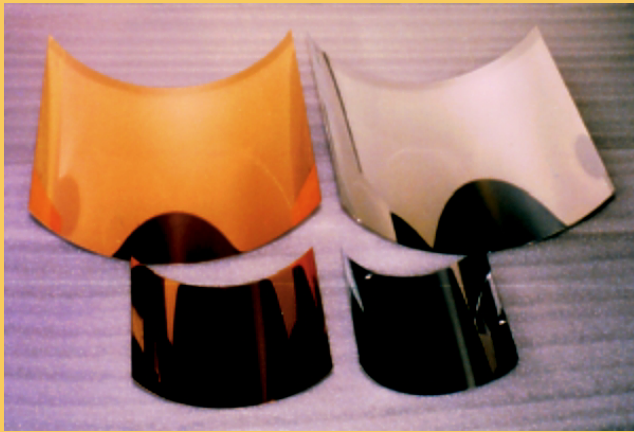
#### **4.4 Hard X-ray Telescope (HXT) Systems**

The fundamental Constellation-X science goals require substantial increases in effective area, energy resolution, and energy bandpass. To measure continuum emission from 10–40 keV with comparable sensitivity to that achieved for spectroscopic measurements below this energy requires a dramatic improvement in signal to noise ratio over current instruments operating in the hard X-ray band. The requisite sensitivity will be achieved with the Hard X-ray Telescope (HXT) by employing focusing optics at these energies for the first time.

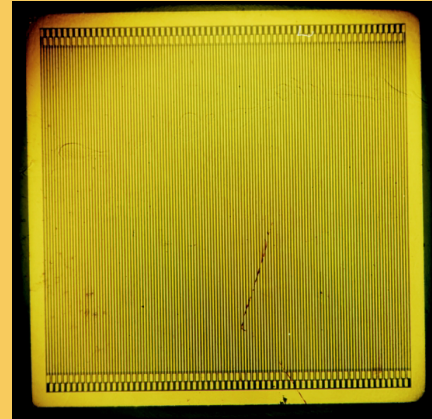
The technical challenge to extending traditional grazing incidence optics into the hard X-ray band is the decrease with energy of the graze angle (the angle of incidence of X-rays on the reflecting surfaces) for which significant reflectivity can be achieved. For a Wolter or conical approximation geometry, the graze angle,  $\gamma$ , on a given mirror shell is related to the focal ratio by  $\gamma = \frac{1}{4} \times r/f$ , where  $r$  is the shell radius and  $f$  is the focal length. If this geometry is maintained, the mirror reflectivity can be extended to high energies either by utilizing small focal ratios or by increasing, for a given  $r/f$ , the graze angle for which significant reflectivity can be obtained. The latter can be achieved by coating the reflective surfaces with graded multilayer structures that operate on the principle of Bragg reflection. This technique provides a large collecting area with very low instrumental background above 10 keV.

To meet the Constellation science goals, the HXT will cover the band pass from 6 to 40 keV (or higher) with an effective collecting area of 1500 cm<sup>2</sup> at 40 keV. It will have a mirror HPD less than 1', a FOV of 12' for energies less than 25 keV and 8' or larger for energies above this. The energy resolution will be better than 10% above 20 keV and 20% below 20 keV. The requisite collecting area can be achieved with four 8.5 meter focal length telescopes on each of four satellites or other equivalent combination.

The HXT mirrors require tightly-nested, light-weight substrates (similar but of smaller radius to the SXT) coated with multilayer structures. The structures contain several hundred layers with each layer consisting of a pair of films with high and low indices of refraction. The layers are typically 25–200 Å thick and must have smooth, sharp boundaries with rms roughness of 3–5 Å. These layers are deposited on the optical surfaces using magnetron sputtering techniques.



Samples of lightweight glass segments that are being studied as optics for the HXT. The segments are formed by “slumping” the glass onto a mandrel with a precise optical surface. The lower pair of segments has a multilayer coating applied.



***CdZnTe detector.***

As for the SXT, two approaches are being developed for producing the mirror shells themselves: one based on replicated integral shells and one based on segmented shells. The segmented shells, manufactured either from glass microsheets thermally formed into conic sections or epoxy-replicated aluminum foils, meet the Constellation-X mass restrictions and are currently at a more advanced stage of development. Integral shells, on the other hand, require advances in replication technology to meet the mass restrictions but offer the potential for substantially better angular resolution, with consequent improvement in signal to noise.

At the focal plane the HXT requires a hard X-ray detector with sub-millimeter spatial resolution. A new generation of high atomic number solid state materials such as CdZnTe and CdTe provide the possibility, when fabricated into pixel detectors, of achieving excellent spatial resolution combined with spectral resolution superior to traditional alkali-halide scintillators (such as NaI) along with high quantum efficiency up to 100 keV. In addition, the compact detector geometry minimizes the shielding mass required to reduce detector background due to cosmic ray interactions in the detector. Even with the use of focusing optics, achieving the background levels of a few  $\times 10^{-4}$  counts  $\text{cm}^{-2} \text{s}^{-1} \text{keV}^{-1}$  requires careful attention to the shield and focal plane design, a critical area of study for the HXT. As an alternate to the less well-developed high-Z solid state detectors, a series of stacked silicon strip detectors is being evaluated as a backup technology.

#### **4.5 Mission Description**

During the Constellation-X Cooperative Agreement Notice (CAN) Study, TRW, and Ball Aerospace teams performed a series of preliminary configuration trades that considered the mission and payload requirements, launch vehicle capabilities, candidate orbits, and costs for the launch vehicles, spacecraft, instrument module, and payload. The mission requirements underpinning these trade studies are given in the baseline mission characteristics table on page 35. This process generated a variety of observatory configurations for each vendor that were ranked by the vendors on the basis of their (effective) collecting area, observing efficiency, mass, time to launch the constellation, development risk, life-cycle-cost, etc.

Below, we present the current GSFC/SAO baseline configuration, as well as the concepts developed by the two spacecraft firms. The final choice for observatory configuration will utilize further mission studies and technology developments to ensure meeting mission requirements and will be based on a balance of overall risk and cost.

Common to the GSFC/SAO, TRW, and Ball approaches was the selection of the mission orbit placing the spacecraft in lissajous orbits around the Sun-Earth L2 point (approximately 1.5 million kilometers from Earth in the anti-solar direction). The L2 orbit was selected by all three studies because it had the fewest observing constraints, an optimum thermal environment, the lowest radiation environment, and simplified spacecraft communications and operations.

Transfer to L2 would be achieved by a lunar flyby with phasing loops to minimize propulsion requirements and obtain a compact lissajous orbit around the L2 point.

#### 4.5.1 GSFC/SAO Baseline Configuration

The current GSFC/SAO baseline observatory configuration consists of four spacecraft (S/C) (configuration as shown in Figure 40), with the S/C consisting of a separate bus and instrument payload module. Each payload module houses one 1.6 m diameter SXT optic/grating and three 40 cm diameter HXT optics. The detectors are deployed using an Extendible Optical Bench (EOB), which is required to package the payload within the launch vehicle fairing yet provide the 10 m focal length deployed on-orbit. The EOB is a four-stage nested trusswork (closed out with MLI blanket) constructed out of a low CTE fiber composite material and is deployed by a stepper motor/pulley/cable system.

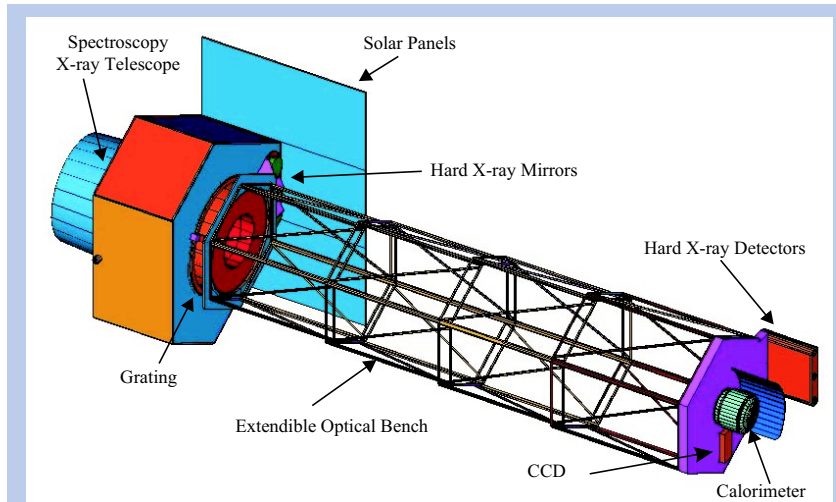


Figure 40. GSFC/SAO Design for four-spacecraft constellation. The Extendible Optical Bench (EOB), shown open here to allow a view of the instruments inside, will be enclosed.

The spacecraft is wrapped around the optics with the solar panels deployed on-orbit. A star tracker and gyro package are also located adjacent to the optics. A cryostat located on the deployed end of the EOB houses the cryogenically cooled detectors for the SXT; the CCD, and HXT detectors are located at this end as well. The joints at the three levels or intersections of the trusses on the EOB as well as the payload connection to the S/C bus are truly kinematic. The detector end of the EOB has a relatively open view to space to accommodate a passive thermal design radiation approach for the cryostat mainshell and CCD detectors. Light-tight closeout is provided above the detector

apertures to the optics by the MLI blanket. The S/C bus is a three-axis-stabilized system with a hydrazine propulsion system to provide thrust for orbit insertion/correction as well as station keeping and momentum management.

The design philosophy for the configuration separates the S/C bus and payload module to minimize cost and complexity associated in the development, design, and qualification of the instruments, and to provide a cost competitive off-the-shelf S/C bus.

#### 4.5.2 TRW Baseline Configuration

The TRW baseline constellation consists of three spacecraft, configured as shown in Figure 41. Each observatory consists of a spacecraft bus based on TRW's GeoLITE satellite design and an ~ 9 m Extendible Optical Bench (EOB) that houses two 1.3 m diameter Soft X-ray Telescopes, six 0.28 m diameter Hard X-ray Telescopes, and the cryogenically cooled detectors. An aperture door/sunshade covers the mirrors during launch and the four telescoping cylinders of the EOB are nested together to fit within the launch vehicle fairing. The spacecraft's solar arrays and high gain antenna are also retracted for launch on a Delta-IV Medium launch vehicle with two strap-on solid rocket motors for additional lift capability.

The TRW observatory design was driven by the mass and collecting area requirements of the payload as well as by the requirements for an 8.4 meter focal length, 65 milli-Kelvin detector, 2" post-facto attitude determination, and simultaneous observations with all observatories.

The total estimated mass of each observatory in the constellation is ~ 3700 kg, and the solar arrays provide ~ 1700 W of electrical power. The observatories communicate with the ground system at X-band via an 0.6 m spacecraft antenna and 11 m ground receiver. Commands are uplinked at 2 kilobits per second and science and engineering data are returned at 1 Mbps.

A bi-propellant propulsion subsystem will meet the transfer orbit maneuver requirements with minimum subsystem mass. The subsystem can be operated in a monopropellant mode (hydrazine only) for station keeping maneuvers to maintain the lissajous orbit. Cryocooling is provided by a modified XRS dewar with shield cooling. A 100 K intercept radiator improves system efficiency and the EOB thermal control is provided by a combination of heat pipes, radiators, blankets, and heaters.

### 4.5.3 Ball Aerospace Baseline Configuration

The Ball design departs significantly from the GSFC/SAO and TRW designs in two key areas. First, it utilizes a fixed optical bench to achieve the required 8.4 m focal lengths rather than an EOB. Second, the design segregates the warm optics and spacecraft bus components from the colder detectors (Figure 42). The Ball approach for the Constellation X mission architecture design includes a suite of telescopes (six spectroscopy and 27 hard X-ray in total) that can be launched on two Evolved Expendable Launch Vehicles (EELV). By virtue of its use of a fixed optical bench, this design also eliminates many of the mechanisms for solar panels, telescope deployments, etc. Shown is a version of the Ball design that packages three soft X-ray telescopes into a single spacecraft.

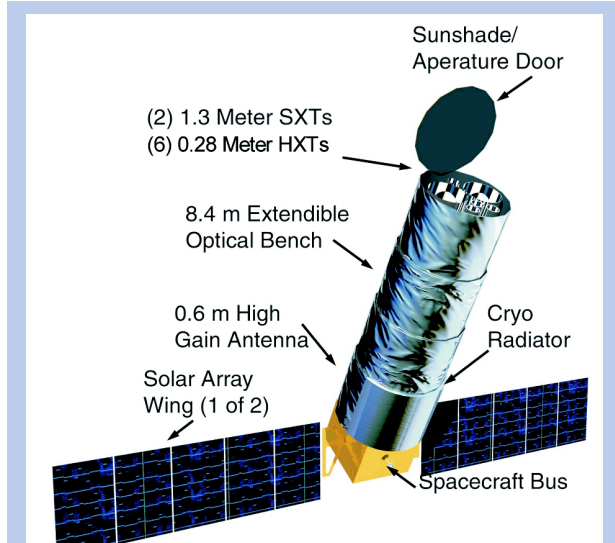


Figure 41. TRW Spacecraft Design.

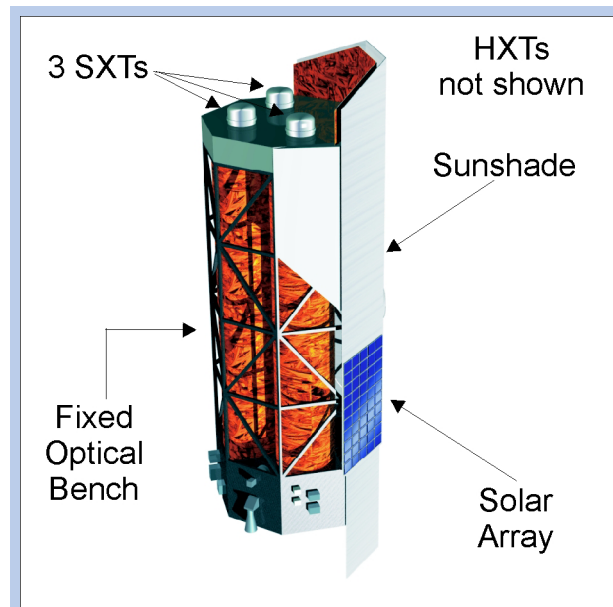


Figure 42. Shown is a version of the Ball design that packages three soft X-ray telescopes into a single spacecraft.

The room-temperature spectroscopy and hard X-ray mirrors are surrounded with the components and structure of the spacecraft bus (this heavy end of the observatory is attached to the launch vehicle). A long (~ 10 m), fixed metering structure/optical bench supports the microcalorimeter, CCDs, and hard X-ray detectors at the appropriate distance from their respective mirrors and gratings. A light-weight solar and thermal shield insulates the detectors from the Sun. The coldest elements (the microcalorimeter cryostats) directly view deep space and are shielded from the Sun and warm spacecraft; other elements (the CCDs, hard X-ray detectors, and their associated electronics) are tied thermally to the appropriate temperature shields. Body-mounted solar panels, thermal shields, and antennas are used in this design. Besides the one-time deployable telescope contamination covers, Ball elected to employ a one-time deployable light shield, to allow enhanced target scheduling flexibility.

The Ball observatory design can be launched on the US Air Force/Commercial sector Evolved Expendable Launch Vehicle (EELV) with a deployment of the full constellation of telescopes requiring two launches.



# References

- Alexander, J., and Balick, B., 1997, *AJ*, 114, 713.  
Antonucci, E., 1989, 104th IAU Colloquium on Solar and Stellar Flares, 121, 31.  
Basko, M., 1978, *ApJ*, 223, 268.  
Boller, Th., Brandt, W.N., Fabian, A.C., Fink, H.H., 1997, *MNRAS*, 289, 393.  
Bregman, J.N., and Houck, J.C., 1997, *ApJ*, 485, 159.  
Cen, R., and Ostriker, J.P., 1998, Astro-ph/9806281.  
Cravens, T. E., et al., 1995, *J. Geophys. Res.*, 100, 17153.  
Cravens, T. E., 1997, *Geophys. Res. Lett.*, 24, 105.  
David, L., Jones, and Forman, 1992, *ApJ*, 388, 82.  
George, I.M., and Fabian, A.C., 1991, *MNRAS*, 249, 352.  
Faber, S.M., and Gallagher, J.S., 1979, *Ann. Rev. A&A*, 17, 135.  
Fabian, A.C., et al., 1998, *MNRAS*, in press (Astro-ph/9803289).  
Fukugita, M., Hogan, C.J., and Peebles, P.J.E., 1998, *ApJ*, 500, 79.  
Gladstone, G.R., et al., 1998, *J. Geophys. Res.*, submitted.  
Guilbert, P.W., and Rees, M.J., 1998, *MNRAS*, 233, 475.  
Hasinger, G., et al., 1998, *A&A*, 329, 495.  
Hellsten, U., Gnedin, N.Y., and Miralda-Escude, J., 1998, Astro-ph/9804038.  
Hughes et al., 1998, *Nature*, 394, 241.  
Krasnopolsky, V.A., 1998, *J. Geophys. Res.*, 103, 2069.  
Koyama, K., et al., 1996, *PASJ*, 48, 249.  
Lightman, A.P., and White, T.R., 1988, *ApJ*, 335, 57.  
Lisse, C. M., et al., 1996, *Science*, 274, 205.  
Lynden-Bell, 1969, *Nature*, 223, 690.  
McClintock, J., 1998, in *Accretion Processes in Astrophysical Systems*, AIP Conf. Proc. 431, 290.  
Madau, P., Ghisellini, G., and Fabian, A.C., 1994, *MNRAS*, 270, L17.  
Metzger, A. E., et al., 1983, *J. Geophys. Res.*, 88, 7731.  
Miyaji, T., et al., 1998, *AA*, 334, L13.  
Morrison, R., and McCammon, 1983, *ApJ*, 270, 119.  
Mosley et al., 1984, *J. Appl. Phys.*, 56, 1257.  
Nandra, K., et al., 1997, *ApJ*, 488, L91.  
Nagase et al., 1994, *ApJ*, 436, L1.  
Nicastro, F., Fiore, F., and Matt, G., 1998, *ApJ* submitted.  
Osterbrock, D.E., Tran, H.D., and Vielleux, S., 1992, *ApJ*, 389, 305.  
Perna, R., and Loeb, A., 1998, *ApJ*, 503, 135.  
Pringle and Rees, 1972, *A&A*, 21, 1.  
Rajagopal, Romani, & Miller, 1997, *ApJ*, 479, 347.  
Reynolds, C.S., and Begelman, M.C., 1997, *ApJ*, 488, 109.  
Reynolds, C.S., 1997, *MNRAS*, 287, 513.  
Savage, B.D., and Sembach, K.R., 1996, *ARAA*, 31, 279.  
Shakura and Sunyaev, 1973, *A&A*, 24, 337.  
Steidel, C.C., et al., 1994, *ApJL*, 437, 75.  
Tanaka, Y., et al., 1995, *Nature*, 375, 659.  
Waite, J. H., Jr., et al., 1994, *J. Geophys. Res.*, 99, 14788.  
Zavlin et al., 1996, *A&A*, 315, 141.



# Acknowledgments

## Facility Science Team (FST) Steering Committee Ex Officio:

Harvey Tananbaum (SAO - Chair)  
Nicholas White (GSFC - Project Scientist)

Jay Bookbinder (SAO - Mission Scientist)  
Frank Marshall (GSFC - Mission Scientist)

## FST At-Large Members:

Keith Arnaud (U. of Maryland)  
Jill Bechtold (U. of Arizona)  
Mitchell Begelman (U. of Colorado)  
Omer Blaes (UC Santa Barbara)  
Joel Bregman (U. of Michigan)  
Blas Cabrera (Stanford U.)  
Claude Canizares (MIT)  
Webster Cash (U. of Colorado)  
Finn Christensen (DSRI - Denmark)  
Oberto Citterio  
(Osservatorio Astronomico di Brera - Italy)  
France Cordova (UC Santa Barbara)  
Arthur Davidsen (Johns Hopkins U.)  
Andy Fabian (Institute of Astronomy - UK)  
Gordon Garmire (Penn State U.)  
Neil Gehrels (GSFC)  
Gabriele Ghisellini  
(Osservatorio Astronomico di Brera - Italy)  
Paul Gorenstein (SAO)  
Charles Hailey (Columbia U.)  
Fiona Harrison (CalTech)  
John Hughes (Rutgers U.)  
Kent Irwin (NIST)  
Neil Johnson (NRL)  
Steven Kahn (Columbia U.)

Richard Kelley (GSFC)  
Hideyo Kunieda (Nagoya U. - Japan)  
James Kurfess (NRL)  
Simon Labov (Lawrence Livermore National Lab)  
Duane Liedahl (Lawrence Livermore Natl Lab)  
Abraham Loeb (Harvard U.)  
Giorgio Matt  
(Universita' degli Studi "ROMA TRE" - Italy)  
Bruce Margon (U. of Washington)  
Stephen Murray (SAO)  
Richard Mushotzky (GSFC)  
John Nousek (Penn State U.)  
Steven O'Dell (MSFC)  
Robert Petre (GSFC)  
George Ricker (MIT)  
Richard Rothschild (UCSD)  
Robert Rosner (U. Chicago)  
Wilt Sanders (U. of Wisconsin)  
Mark Schattenburg (MIT)  
Eric Silver (SAO)  
Michael Shull (U. of Colorado)  
Leon Van Speybroeck (SAO)  
Caroline Stahle (GSFC)  
Melvin Ulmer (Northwestern U.)  
Martin Weisskopf (MSFC)

**Technology Development Leader:** Robert Rasche

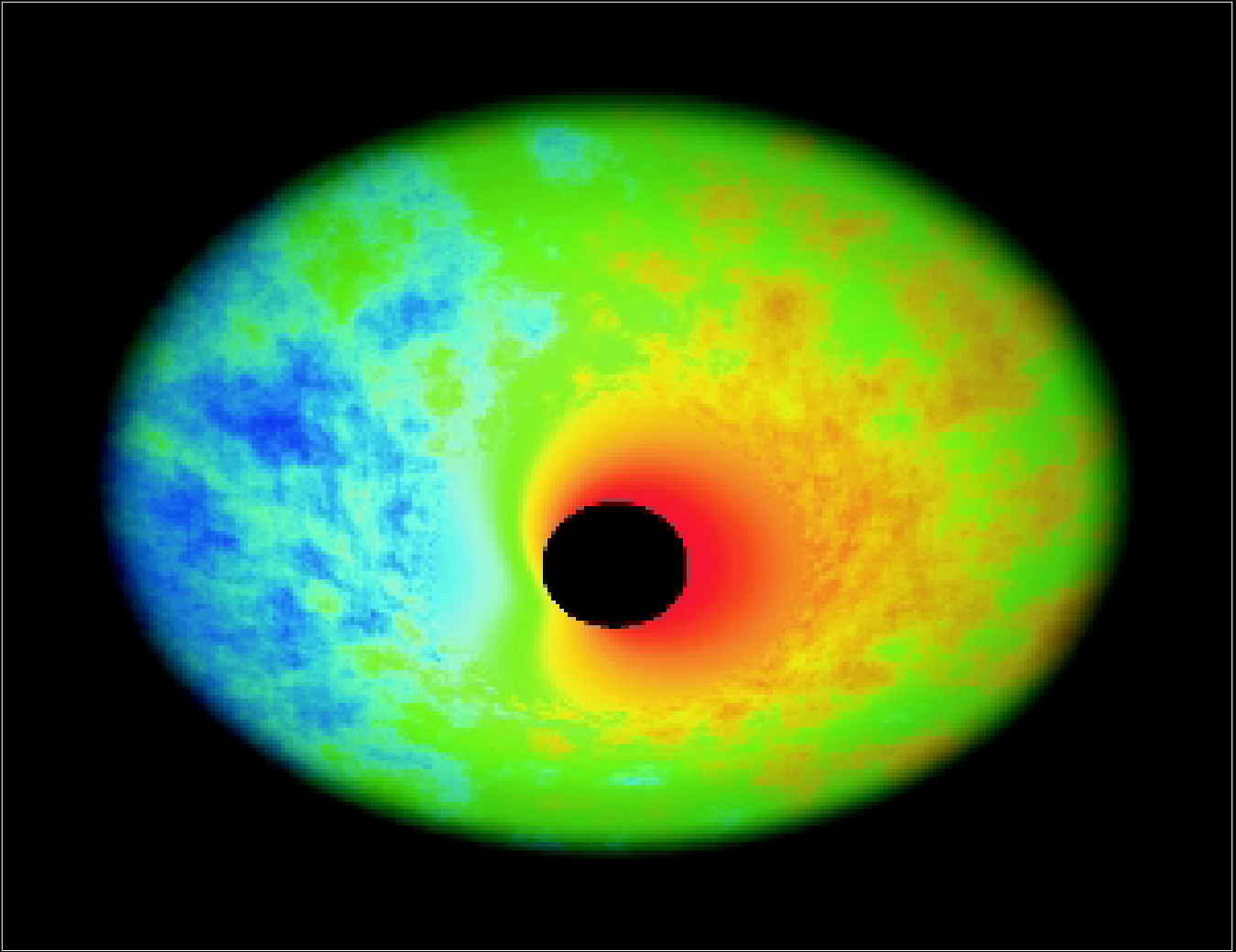
**Integral Product Team Leads:** Fiona Harrison (HXT), Steven Kahn (CCD/Grating), Richard Kelley (Calorimeter), Leon Van Speybroeck (Spectroscopy X-ray Telescope)

**Science Panel Chair (France Cordova) and Science Panel Leads:** Keith Arnaud, France Cordova, Andy Fabian, John Hughes, Richard Mushotzky, John Nousek, Robert Rosner, Martin Weisskopf, Nicholas White

We also thank John Arabadjis, Keith Arnaud, Jay Bookbinder, Niel Brandt, Joel Bregman, Eugene Churazov, France Cordova, Steve Drake, Ronald Elsner, August Evrard, Andy Fabian, Ian George, Randy Gladstone, Fiona Harrison, John Hughes, Una Hwang, Keith Jahoda, Steve Kahn, W.S. Lewis, Duane Liedahl, Abraham Loeb, Mike Loewenstein, Greg Madejski, Smita Mathur, Giorgio Matt, Jeff McClintock, Richard Mushotzky, Hagai Netzer, Fabrizio Nicastro, John Nousek, George Pavlov, Robert Petre, Chris Reynolds, Wilt Sanders, Mike Shull, Steve Snowden, Caroline Stahle, Tod Strohmayer, Hunter Waite, Diana Worrall, and Slava Zavlin, as well as the GSFC/SAO, Ball Aerospace, and TRW study teams for their contributions to this document.

**Editors:** Jay Bookbinder, Harvey Tananbaum, Patricia Tyler, Azita Valinia, Kim Weaver, and Nicholas White.





*This simulated image (made by Ben Bromley at Harvard-Smithsonian Center for Astrophysics) shows what the accretion disk around a black hole might look like. The distortions of time and space by the intense gravity of the black hole and motion of the material at close to the speed of light, cause red and blue shifting of the emission (the color indicates the relative frequency shift of observed photons). The disk is turbulent and located around a Schwarzschild (non-rotating) black hole. It extends from  $2 R_g$  (near the event horizon) to about  $12 R_g$ , and is seen at an inclination angle of 30 degrees. At large radii the disk material is on circular orbits, but at a radius of  $6 R_g$ , these orbits become unstable and the disk material begins a “free fall” orbit. Constellation-X will be able to measure distortions of time and space through distortions of the iron K line and thus will determine both the mass and spin of the black hole. By probing this close to the black hole Constellation-X may also be able to test the validity of General Relativity in the strong gravity limit.*

